GeorgiaInstitute of Technology

Research Grant GTRC-03-01/2552-GT

"Enhancing the Design Process for Complex Space Systems through Early Integration of Risk and Variable-Fidelity Modeling"

Final Report

Submitted to:

Leslie Filipiak
National Institute of Aerospace
144 Research Drive
Hampton, VA 23666
Phone (757) 766-1536
leslie@nianet.org

Dr. Robert Whitehead
National Institute of Aerospace
144 Research Drive
Hampton, VA 23666
Phone (757) 766-1466
bobw@nianet.org

Dr. Thomas Zang
NASA Langley Research
Center
Hampton, VA 23681
Phone (757) 864-2307
thomas.a.zang@nasa.gov

31 March 2005

Principal Investigator: Dr. Dimitri Mavris
dimitri.mavris@ae.gatech.edu

Project Coordinator: Dr. Jan Osburg
jan.osburg@asdl.gatech.edu

Graduate Research Assistants:
Bjorn Cole, Dominic DePasquale, John Sebastian, Bryan Tisinger

ASDL

Aerospace Systems Design Laboratory
Guggenheim School of Aerospace Engineering
Georgia Institute of Technology
Atlanta, GA 30332-0150

Contents

Research Grant GTRC-03-01/2552-GT – Final Report – March 2005

1 Executive Summary

An important enabler of the new national Vision for Space Exploration is the ability to rapidly and efficiently develop optimized concepts for the manifold future space missions that this effort calls for. The design of such complex systems requires a tight integration of all the engineering disciplines involved, in an environment that fosters interaction and collaboration.

The research performed under this grant explored areas where the space systems design process can be enhanced: by integrating risk models into the early stages of the design process, and by including rapid-turnaround variable-fidelity tools for key disciplines.

Enabling early assessment of mission risk will allow designers to perform trades between risk and design performance during the initial design space exploration. Entry into planetary atmospheres will require an increased emphasis of the critical disciplines of aero- and thermodynamics. This necessitates the pulling forward of EDL disciplinary expertise into the early stage of the design process. Radiation can have a large potential impact on overall mission designs, in particular for the planned nuclear-powered robotic missions under Project Prometheus and for long-duration manned missions to the Moon, Mars and beyond under Project Constellation. This requires that radiation and associated risk and hazards be assessed and mitigated at the earliest stages of the design process. Hence, RPS is another discipline needed to enhance the engineering competencies of conceptual design teams.

Researchers collaborated closely with NASA experts in those disciplines, and in overall space systems design, at Langley Research Center and at the Jet Propulsion Laboratory. This report documents the results of this initial effort.

Research Grant GTRC-03-01/2552-GT – Final Report – March 2005

2 Introduction

The new National Space Policy, as announced by President Bush on January 14, 2004, establishes a vision for the sustained human and robotic exploration of the solar system [1]. An important enabler of this Policy is the ability to rapidly and efficiently develop optimized concepts for the manifold future space missions that this vision calls for. The design of such complex systems requires a tight integration of all the engineering disciplines involved, in an environment that fosters interaction and collaboration. An enhanced national capability for the aerospace R&D community is needed to permit a true national exploration initiative with the greatest possible efficiencies and lowest risk.

The research performed under this grant explored areas where the space systems design process can be enhanced: by integrating risk models into the early stages of the design process, and by including rapid-turnaround variable-fidelity tools for the key disciplines of aero- and thermodynamics for entry, descent and landing (EDL) as well as radiation protection and shielding (RPS).

2.1 The Need for Integrating Risk, EDL and RPS Disciplines

The Vision for Space Exploration, with its focus on exploration, will require an increased amount of planetary landing missions, which contain additional risks to be managed and additional disciplines and technologies to be integrated.

Enabling early assessment of mission risk will allow designers to perform trades between risk and design performance during the initial design space exploration. Entry into planetary atmospheres will require an increased emphasis of the critical disciplines of aero- and thermodynamics. This necessitates the pulling forward of EDL disciplinary expertise into the early stage of the design process.

Another discipline, radiation, can have a large potential impact on overall mission designs, in particular for the planned nuclear-powered robotic missions under Project Prometheus and for long-duration manned missions to the Moon, Mars and beyond under Project Constellation. This requires that radiation and associated risk and hazards be assessed and mitigated at the earliest stages of the design process. Hence, RPS is another discipline needed to enhance the engineering competencies of conceptual design teams.

Incorporating disciplinary knowledge at variable levels of fidelity will benefit the process by enabling the use of subsystem models with disparate fidelity levels, and allow the designers to model relevant new technologies at appropriate levels of fidelity.

Risk, EDL and RPS disciplinary competencies are available at NASA's Langley Research Center (LaRC), which supported the research documented in this report. On the integration side, the Jet Propulsion Laboratory's "Project Design Center" (PDC; described below) provided an example for the integrated conceptual systems design environments that will
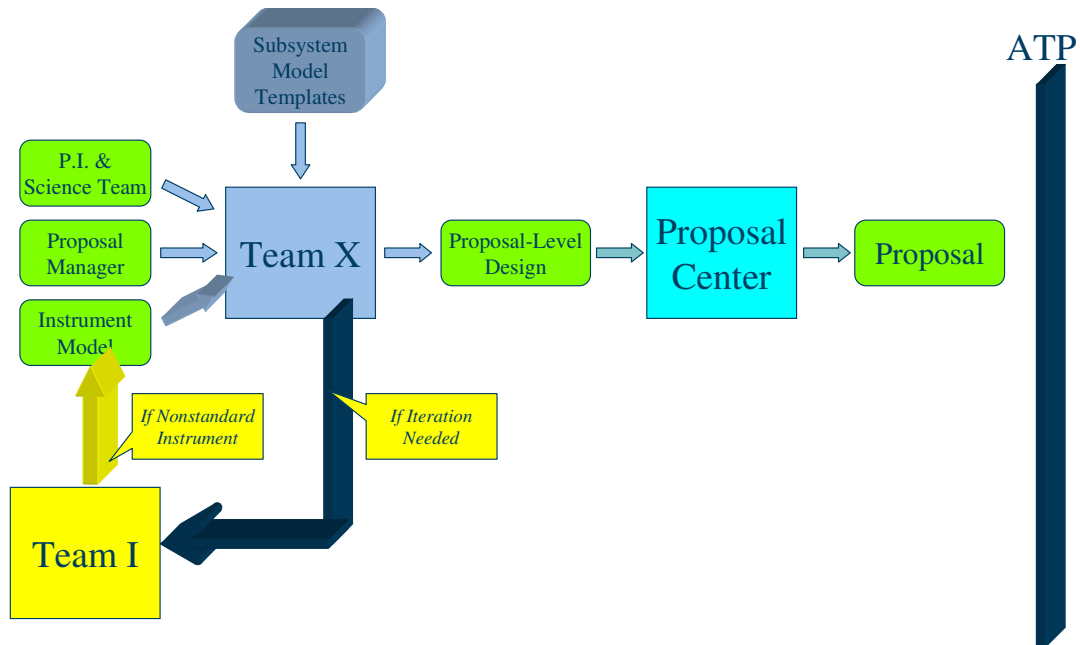
Figure 1: JPL PDC Elements

Integration of these competencies into the early design process, in a manner that addresses risk and incorporates variable-fidelity, will enhance NASA's capability for rapid-turnaround design of new missions and thereby support the Vision for Space Exploration's renewed spirit of discovery.

2.2 Integrated Design Environment

The Jet Propulsion Laboratory's (JPL) "Project Design Center" (PDC) provides a prime example of such a capability. It is chartered to [2]:

- "Improve the speed and quality of JPL's new mission concepts"

- "Create a reusable study process with dedicated personnel, facilities, equipment, procedures, and tools to enhance proposal generation"

- "Develop a database of initial mission requirements that can be easily updated and electronically transferred for use in subsequent project phases"

- "Develop mission generalists from a pool of experienced engineer"

The PDC design team ("Team X") members represent the engineering disciplines related to a mission, in addition to a team leader and a documentation specialist. A separate team ("Team I") addresses science instrumentation requirements and provides an instrumentation model. Figure 1 shows the organization of the PDC process.

PDC design projects last between one and two weeks. The output from a PDC project is an electronic report containing system and subsystem descriptions, equipments lists, mass and power budgets, and mission cost estimate. The PDC is also

used to review existing proposals; such reviews last one or two days and result in abbreviated reports.

The JPL PDC, therefore, represents an excellent "platform" on which to validate research advancements to enhance the space systems design process.

2.3 Research Activities

The researchers investigated and developed the enhancements described above in close coordination with members of the PDC space mission design team and the discipline experts at LaRC, to enhance the benefit of this research to NASA. Research in each of the focus areas was performed in three phases:

Phase 1: Familiarization with the PDC process, with current approaches to risk and variable fidelity modeling, and with the disciplinary approaches of EDL/RPS engineering at LaRC and PDC

Phase 2: Development and formulation of a strategy to integrate EDL/RPS (including new approaches to risk and variable fidelity modeling where indicated) into the PDC process

Phase 3: Demonstration of the strategy at the proof-of-concept level, to include generating models of advanced EDL/RPS technologies

The coordination of the effort included extended on-site visits to LaRC and PDC. This report documents the approach and results for the four areas that were investigated:

◇ Thermal analysis for EDL

◇ Aerodynamic analysis for EDL

◇ Risk analysis for EDL

◇ Radiation protection and shielding issues for planetary missions

In three of the four focus areas, the researcher's background in robust design, rapid-turnaround simulation methodologies, and modeling of disciplinary tools in a manner suitable for the conceptual and systems design process was utilized to its full extent. In the following, a brief introduction to that approach is provided.

2.4 Modeling and Analysis Methodology

The status quo for the modeling and simulation approach used during the earliest phases of design frequently is based on 0th-order spreadsheets featuring empirical equations and table lookups. This sacrifices analytical fidelity in favor of rapid turnaround and ease of linking among the different disciplines of the system under design. Traditional higher-order methods are generally considered to be too slow and cumbersome for the rapid iteration and integration of design cycles that define capability-based design. However, 0th-order methods are generally applicable only to systems that fall within the boundaries of established design experience, where

historical precedent can provide the simple equations utilized to calculate system metrics.

For design tasks transcending those boundaries, a new approach is required that enables rapid-turnaround design space exploration based on the physics of the problem under consideration. Capturing the essence of higher-fidelity tools through creation of surrogate models enables the application of probabilistic techniques to capture uncertainties and provide the designers with rapid visualizations of the design space and its sensitivities. Metamodels are employed to capture the essence of higher-fidelity tools while keeping computational effort to a minimum, which enables running the large number of analysis cases necessitated by the stochastic approach.

With the advent of economical and massive-parallel computer power, it is now possible to create metamodels efficiently. By using computing tools to predict performance for a wide array of alternatives, it is feasible to probe the entire design space and elicit some familiarity with designs that have never existed. While computing a CFD solution in hours rather than weeks is now considered "rapid analysis," this is still too slow to run quick, off-the-cuff "what if" scenarios and trades.

One alternative may be to link all the analyses together with an optimizer, but this cuts the designer out of the loop, and the knowledge about issues that were not modeled with him. The other possibility is to regress data created by high-fidelity disciplinary tools. One regression technique is the response surface methodology. It is considered an enabling technology for rapid and well-informed design trade-offs. There are two main questions it seeks to address:

◊ What is the minimum amount of data that must be collected in order to understand the design space?

◊ Can this information be contained in an easy-to-use, flexible format?

The first of these questions is addressed by the Design of Experiments (DoE) approach, which is at the heart of the modeling and analysis methodology presented here. Each run of the high-fidelity disciplinary tool is considered an "experiment", and these experiments are designed to span the design space and do so evenly, with no false correlations between variables being introduced, and with a minimum number of experiments and thus high-fidelity tool executions, i.e. computing cost and time. For a given number of design variables, the DoE will prescribe a set of trials to be undertaken at various settings of these variables. For computational analysis, DoE tables are used to generate a sequence of input files to be run in a batch.

The second issue is solved through the use of Response Surface Equations (RSEs). RSEs take the data generated by executing the DoE runs and attempt to determine co-efficients *bij* in a polynomial equation, most frequently a quadratic form:

$$R = b_0 + \sum_{i=1}^{k} b_i x_i + \sum_{i=1}^{k} b_{ii} x_i^2 + \sum_{i=1}^{k-1} \sum_{j=i+1}^{k} b_{ij} x_i x_j$$

Here, the x terms are the design variables and the R term is the desired response, which could be cost, lift, thrust, risk or whatever the designer wishes to estimate.

Thus, each RSE is a simple finite polynomial series, which can be evaluated in microseconds by a computer. Assuming this function approximates the underlying data well within a given validity range of the design variables, it provides the desired capability to perform flexible trades, in real time if the designer desires.

A statistical software tool is required in order to generate the responses. The researchers have successfully used the commercial off-the-shelf software JMP for this purpose [3]. The data points generated using the respective higher-order disciplinary tool are entered into JMP in tabular form. JMP uses least squares regression to obtain its "best fit model", which minimizes the sum of the squares of the differences between the data points (actual data from higher order model) and its best fit-model (predicted data from JMP best-fit line). Higher order terms can be added to the response surface equations if the second order model does not capture all of the higher order trends.

Because the response surface equations are a metamodel (a model of a model), it is of vital importance that they are highly accurate. JMP has tools built in to determine and asses the accuracy of the model, and if necessary, improve the best fit models. The first tool is an actual by predicted plot, which graphs the actual points from the high-fidelity runs versus the points predicted by JMP's response surface equation (for an example, see Figure 16). A good actual by predicted plot has the dots (cases) as close to the line as possible. The solid red line represents a perfect fit, and the dotted red lines represent the 95% confidence intervals.

Another tool is the residual by predicted plot. The residual is the error in the fitted model, which is the difference between the actual value of each observation and the value predicted by the fitted model. A good residual by predicted plot has a random scatter of points, which is illustrated for a C_L fit in Figure 15.

Once the model is determined to be a good fit, the parameter estimates for each response are copied from JMP to Microsoft Excel. The parameter estimates are terms which are used to multiply their respective design variables or combination of design variables to obtain an estimate for the response. These estimates are essentially the constant coefficients used in an equation which multiply the variables in order to calculate the "answer", which are the responses, or metrics. The designers then use the equations in Excel to calculate the estimates for their metrics of interest.

This approach has been applied for the thermal, aerodynamics and RPS tasks.

3 Thermal Task

3.1 Introduction

The entry phase of an interplanetary vehicle into a planet's atmosphere begins with the vehicle slowing down from orbital or higher speeds using aerodynamic drag. One of the consequences of this rapid deceleration is that the kinetic energy of the entry vehicle is dissipated via thermal energy or heat. This thermal energy is high enough to severely damage the entry vehicle if it isn't properly protected. A Thermal Protection System (TPS) is required to protect an entry vehicle from this thermal energy. There are two classes of TPS: reusable TPS and ablative TPS. Reusable TPS are preferred for milder entry conditions (Heat loads < 75 W/cm^2) and do not involve mass or property changes. Ablative TPS, on the other hand, are designed to accommodate high heating rates and heat loads. Furthermore, ablative TPS goes through phases changes and mass losses [4].

TPS sizing for an entry vehicle is an important step when sizing the entry system. The atmospheric entry of an entry vehicle is one of the most demanding parts of the mission and therefore the success of the TPS crucial. The TPS must sufficiently insulate the vehicle from the heat while not adding significantly to the overall weight of the entry system. The TPS sizing, therefore, is a complicated trade between providing more insulation at the cost of increasing the system weight. Looking back on past missions, it is evident that TPS can account for a significant percent of the entry system weight. Figure 2 below shows a plot of TPS mass fraction vs. total heat load. Notice that, depending on the mission, the mass fraction of the TPS can range anywhere from 10% on Mars entry vehicles up to 40% on Jupiter entry vehicles [5].
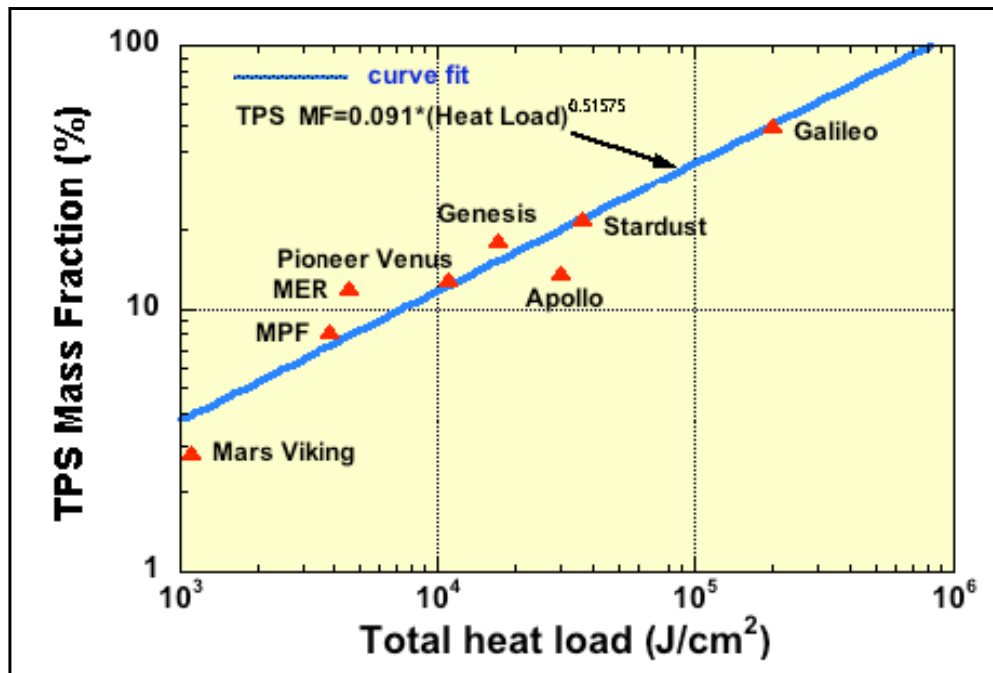
Figure 2: TPS mass fraction for different planetary entry systems

With such a significant mass fraction, it is important that the design process at the preliminary level capture as much information regarding the TPS sizing process as possible. However, since it is still in the preliminary design stage, rapid-turnaround analysis tools are necessary to allow for a quick iteration on a design point. This is the challenge that the thermal task section of this report will address: investigating a preliminary TPS sizing tool that will provide both reliable and rapid analysis.

Before discussing the rapid turnaround TPS sizing tool, the more detailed tools must be understood. Two of the primary TPS sizing codes used by NASA are Charring Material thermal response and Ablation (CMA) and Fully Implicit Ablation and Thermal analysis program (FIAT). CMA and FIAT are both high fidelity, complex numerical solvers that model ablative TPS. These codes account for all the physical and chemical processes occurring in the TPS material such as surface recession rates, in-depth pyrolysis, and charring effects [6]. Both CMA and FIAT have been used to size TPS for past missions. However, the price for such high fidelity tools is execution time. The input files for these codes can be as large as 30 pages and a significant amount of time is necessary to ensure a single design point will be accurately modeled. Such time intensive analysis codes, though accurate, are no longer a benefit during the preliminary stages of an entry system design when the design is still rapidly evolving.

3.2 Approach

As mentioned earlier, a rapid TPS sizing tool will be investigated within the thermal task section. The tool selected for this type of analysis is a subroutine contained within a

thermal analysis software called SINDA. SINDA can be described as a general-purpose thermal network analyzer. It has the capability of solving both finite difference and finite element equations [7]. A simple ablation subroutine called ABLATE exists within SINDA that models one-dimensional ablative thermal protection systems. This routine is referred to as "simple" because of how it approximates ablation.

Actual ablation is a complex interaction of heat and mass transfers from the ablative layer to the hypersonic flow. Figure 3 shows a typical cross section of a TPS with the resulting interactions during hypersonic entry. The boundary layer is through which the heat loads are transferred into the entry vehicles via convection and radiation. The char layer that sits above the ablative material (virgin material) is the result of ablative material that has already undergone pyrolysis. Conduction takes place through the char layer and interacts with the virgin material as well as the pyrolysis zone. Pyrolysis can best be described as the internal decomposition of the solid that releases gaseous species [9]. The pyrolysis zone is the level at which the material ablates away. These changes in mass and states create a complex environment in which ablation takes place. The earlier mentioned codes, CMA and FIAT, are complex enough to thoroughly handle these interactions.
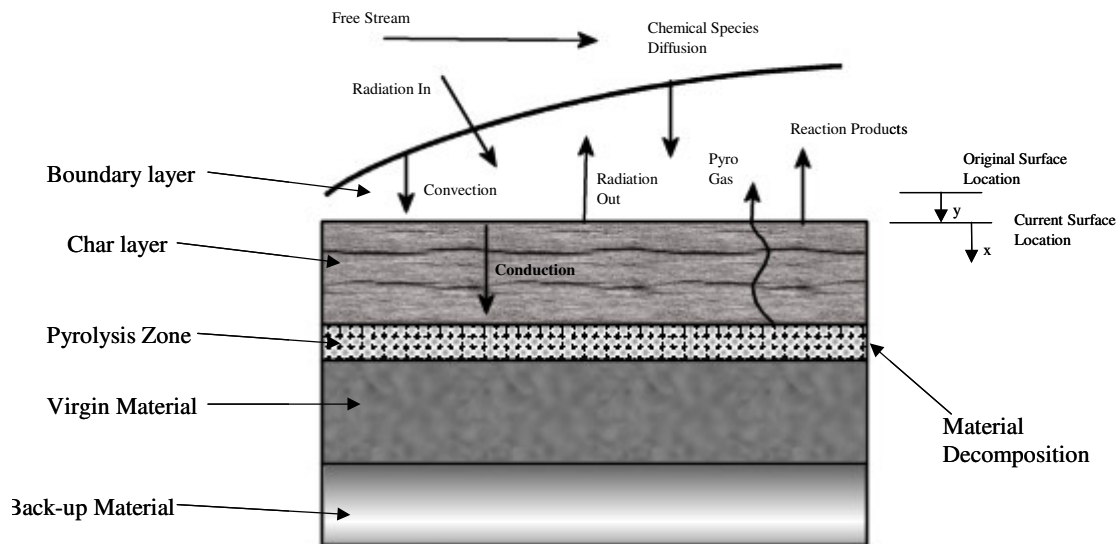
Figure 3: Cross-sectional view of the ablation process [8]

The simple ablation tool ABLATE, however, does not model charring and pyrolysis affects. Instead, it approximates complex ablation characteristics using two major parameters: heat of ablation and temperature of ablation. Heat of ablation is a data correlation parameter derived from steady-state ablation cases. Temperature of ablation is the temperature at which surface recession begins. It should be noted that these two parameters are the primary parameters that ABLATE uses to approximate the complex numerial calculations that CMA and FIAT execute for ablation cases. With these

parameters ABLATE determines the surface recession rate and ablates the material away accordingly. Table 1 outlines the comparison between the high fidelity tools CMA/FIAT and the low fidelity tool ABLATE.

Table 1: Ablation tool comparisons

CMA/FIAT	ABLATE
Complex numerical solver	1-D finite-difference model
Computes surface recession rate, in-depth pyrolysis, and charring effects	Computes surface recession, but does not include charring effects
30-pages input data	Simple input file
High fidelity code	Low fidelity code
Used for sizing existing missions	Not yet correlated

Additionally, the ABLATE tool models ablative material in only one dimension. This is satisfactory because typical ablative materials have low thermal conductivity coupled with small aspect ratios. Basically, this states that temperature gradients are assumed to exist only within the thickness dimension. Figure 4 shows a schematic of how an ablative layer is discretized into nodes and conductors within ABLATE. Each layer within the ablative material is represented by a single linear conductor and a single node. Once the intial thermal network is created, the heat load is modeled as a boundary node that operates on the first node and conductor representing the first ablative layer in the 1-D network (G1 and N1 in Figure 4). Based on the appropriate heat of ablation and temperature of ablation parameters, these ablative layer nodes will begin to ablate away and eventually collapse. At the end of the transient case, the ABLATE tool will output the thickness of the remaining ablative layer.
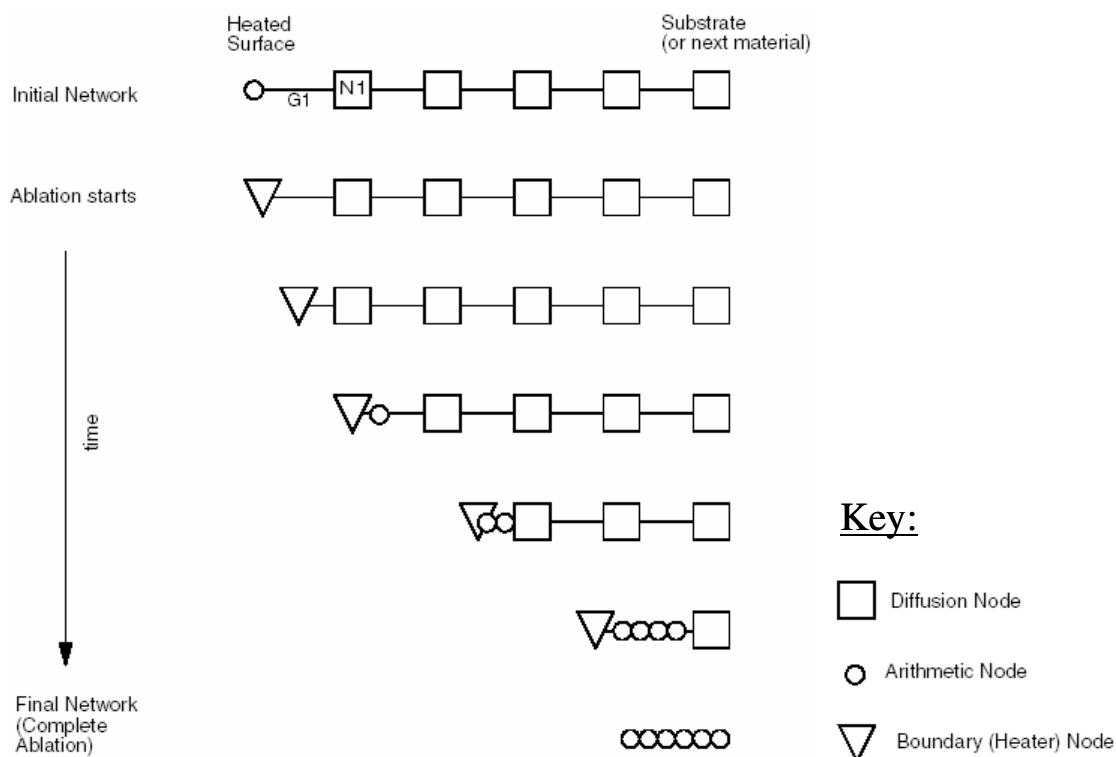
Figure 4: ABLATE 1-D approximation of ablation [7]

However, as of yet, the ABLATE tool has not been correlated with an exisiting code for accuracy. Such a correlation would be useful to show if the ABLATE tool's approximations for the ablation process are satisfactory enough to use as a preliminary design tool. In order to demonstrate that, the ABLATE tool was setup to correlate a sample ablation case that has been successfully run with CMA. Since the ABLATE tool is a low fidelity tool, the goal is not to have ABLATE's results match up exactly with CMA's, but rather see how close ABLATE's results get to CMA's by approximating certain ablation parameters. The sample case selected is the Earth Entry Vehicle (EEV) from the Mars Sample Return mission. The goal of the EEV is to safely transport Mars samples through Earth's atmosphere and land at a recoverable location on the surface of Earth. A 12-mm layer of carbon phenolic is the ablative material chosen for forebody of the entry vehicle.

3.3 Implementation

Setting up the ABLATE tool involves gathering certain details regarding the heat loads that the EEV would experience as well as certain properties of the ablative material to be modeled. The heat loads can be provided to ABLATE as an array of heat flux (convective plus radiative) vs. time. This allows ABLATE to accommodate heat load

analyses from another tools. ABLATE also accommodates temperature-varying conductance and specific heats for the ablative material. Temperature-varying conductance and specific heats will have a significant effect on how the ablative material responds to the heat loads.

As mentioned above, ABLATE can incorporate heat flux gradients with respect to time. However, these heat flux values are stagnation-point heating that only the nose of the forebody experiences. Moreover, the heat flux is not constant across the entire forebody due to shape of the entry vehicle and its entry angle. In order to accommodate the heat flux variations across the forebody a spatial factor will be used. Therefore, the stagnation-point heat flux is multiplied by a spatial factor, which is a function of radial distance. In order to determine the spatial factors, two boundary conditions across the forebody must be established: nose and shoulder. The interior spatial factors are calculated by first dividing the heat flux at the interior by flux at the two boundary conditions. Then these interior spatial factors are interpolated between 1.0 and the above ratios. Figure 5 has a graph that shows the results of this interpolation. Notice that the spatial factor decreases as it moves away from the stagnation point except at the shoulder of the forebody where it increases.
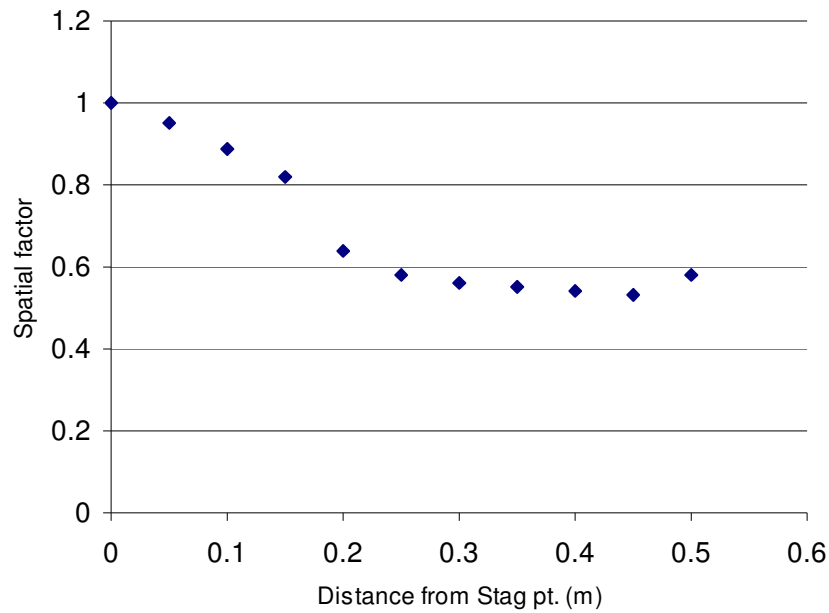

Figure 5: Spatial factor values across the forebody

As mentioned earlier, heat of ablation and temperature of ablation are two parameters that ABLATE uses that CMA doesn't. These two parameters are characteristics of the ablative material itself. However, after consulting the TPSX website, a site that catalogs different ablative materials and their properties, it was

discovered that these parameters weren't listed for carbon phenolic. Further investigation of alternative resources led to the same result. The temperature of ablation was eventually assumed as the temperature at which surface recession begins. In the case of carbon phenolic, an initial assumption of 2000K was used. For the heat of ablation, there was certain doubt as to the appropriateness of using this parameter. Apparently, the heat of ablation parameter is commonly misunderstood. Heat of ablation is not a material property but rather a data correlation parameter [10]. In addition, this correlation parameter is valid only for steady-state ablation conditions. Therefore, for the EEV case, which is a transient ablation process, the heat of ablation parameter does not exist.

However, without a heat of ablation input, the ABLATE tool will not work. Therefore, a guess value must be used for the tool to successfully run. This approach changes how the ABLATE code will be correlated. Originally, instead of comparing the results from CMA and ABLATE and investigating how accurate the approximation is, now the approach will be to identify the values for the heat of ablation and temperature of ablation that will yield results similar to CMA's. The primary results from CMA that will be used in the correlation are final surface recession, surface recession vs. time and bondline temperature vs. time. As the term suggests, surface recession refers to how much of the ablative material will ablate away after experiencing the entry heating loads. The bondline temperature refers to the temperature of the structure beneath the TPS layer that is being protected. Ideally, the goal of the TPS is to prevent the bondline temperatures from exceeding a certain temperature threshold in order to maintain structural integrity. For the EEV, if the bondline temperature rises above 370° C the case is considered a failure [11]. So for the ABLATE correlation, both the surface recession and bondline temperature results from CMA will be used.

Up until now, the analysis tool described works with an input file that numerically "describes" the entry vehicles to be analyzed. However, during preliminary analysis the entry vehicle's geometry will rapidly change as the design iterates. As these changes occur, the input file will have to be constantly updated to incorporate the new geometry and accurately model ablation. One approach to accommodate changing geometry would be creating a parametric geometry model of the entry vehicle. As certain characteristics of the entry vehicle change during preliminary design, such as height, diameter, and cone angle for example, the parametric geometry model can be quickly altered to match the current design. This type of environment coupled with the ABLATE tool would allow the user to perform multiple ablation analyses with different geometries relatively quickly.

In order to create a parametric geometry environment the software Thermal Desktop is used. Thermal Desktop is a graphical, CAD-based interface to SINDA. This allows the user to create geometries within Thermal Desktop and run thermal analyses on these geometries using SINDA's capabilities. Thermal Desktop has the capability to treat the dimensions of the geometry as variables so parametric changes to the geometry are possible.

Using the parametric capabilities of Thermal Desktop, a generic entry vehicle will be created. The majority of the dimensions of this vehicle will be defined as variables. The major dimensions are the entry vehicle's height, diameter, conical angles, and forebody ratio. The forebody ratio is defined as the percentage of the height that is comprised of the forebody. Figure 6 shows this generic entry vehicle with the dimensions defined. The nose radius and the backplate were defined as functions of the height, diameter and forebody ratio.
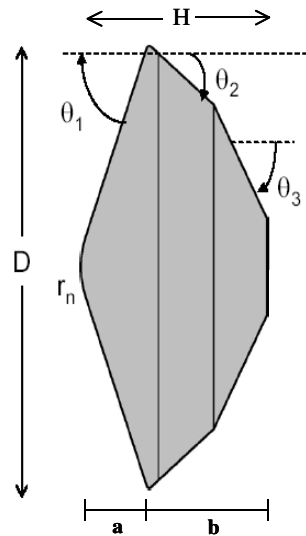

Figure 6: Generic entry vehicle characterized by variables

In the end, the integration of both the numerical ABLATE analysis tool with the parametric geometry environment in Thermal Desktop is the final goal of the thermal task. Within Thermal Desktop, the ablative layer can be characterized similarly to the way it was done within SINDA. Therefore, Thermal Desktop will assign the forebody surface with a 12-mm thick carbon phenolic ablative layer. In addition, a heat load can be applied to the geometry of the entry vehicle simulating the entry conditions. Once the problem has been setup in Thermal Desktop, analyses can be run for different geometries by quickly changing the parametric geometry.

3.4 Demonstration

The EEV case was setup as it was described in the implementation section. The dimensions of the EEV are as follows: 1.0 meter diameter and 0.3 meter height. Figure 7 shows a cross-section of the designed entry vehicle. The Mars sample is contained within the impact sphere. Around the impact sphere is carbon-carbon structure that is uniquely shaped so that as the entry vehicle enters the Earth's atmosphere, aerodynamic drag will force the vehicle to point in the preferred direction. The preferred direction would be the forebody of the EEV facing forward and into the flow field. As mentioned earlier, the forebody is coated with carbon phenolic, the vehicle's primary heat shield.
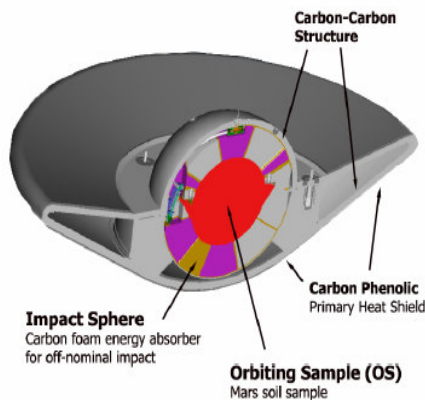
Figure 7: Cross-section of Earth Entry Vehicle

First, the ABLATE code was run independently of Thermal Desktop, in order to have an initial working case. The case ran 11 different ablation scenarios along the length of the EEV corresponding to the 11 different spatial factors. Within minutes, ABLATE outputted the results of the EEV ablation. The outputs included ablative layer recession (for stagnation point as well as remaining spatial factors) and bondline temperature, both as functions of time.

However, ABLATE's initial results differed greatly from CMA's. This was expected because the two parameters, heat of ablation and temperature of ablation, were not accurately set. Both were initially estimated. Now with a successfully run case, ABLATE's results will be matched with CMA's and heat of ablation and temperature of ablation parameters will be back-solved. This process involved running numerous cases of ABLATE in order to understand how the two parameters affected the ablation results. Interestingly enough, from the multiple iterations it was noted that these parameters are indeed dependent on each other. Therefore, it wasn't a simple task of fixing each parameter individually.

After multiple iterations, ABLATE's final results are shown in Figure 8 and Figure 9. Since the goal was to match results from both tools, it shouldn't be a surprise that the data from both results are very similar for the stagnation-point surface recession vs. time (Figure 8). The bondline temperature vs. time graph in Figure 9, however, shows quite different results for both tools. After 50 seconds into the analysis, the results diverge from each other. Furthermore, the trends are not similar. CMA's results show bondline temperature increasing quickly to about 220° C and then slowly decreasing to below 200° C after 350 seconds. These are expected results because peak heating for entry vehicle occur between 0 and 50 seconds. The ABLATE results for bondline temperature, however, shows temperature continuing to increase from 0 to 350 seconds and peaking at 440° C at 350 seconds.

Thickness vs. Time
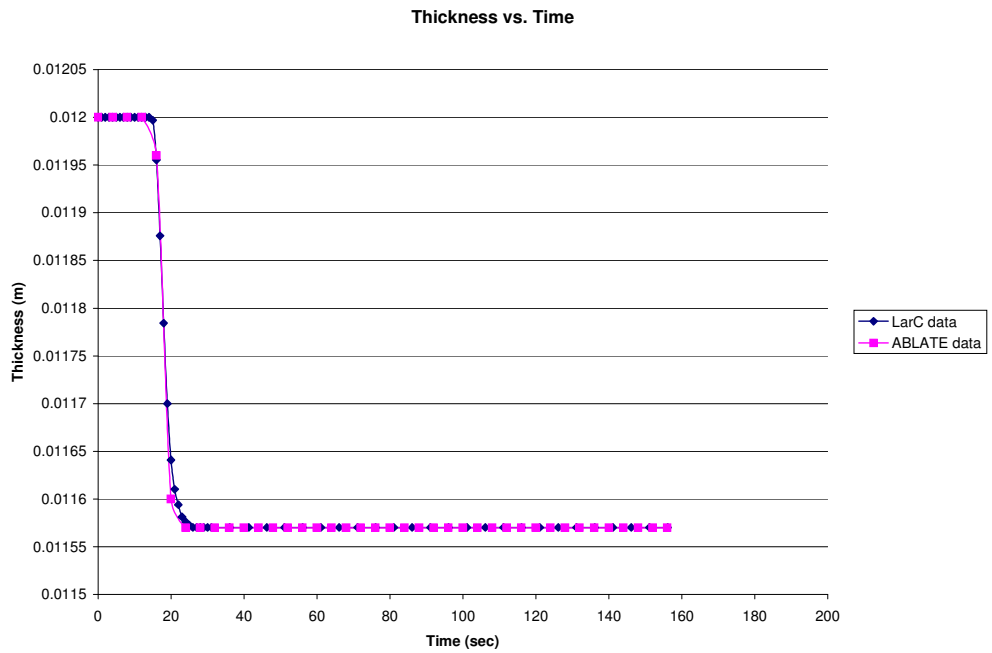
Figure 8: Stagnation point surface recession of carbon phenolic vs. time

Bondline Temperature
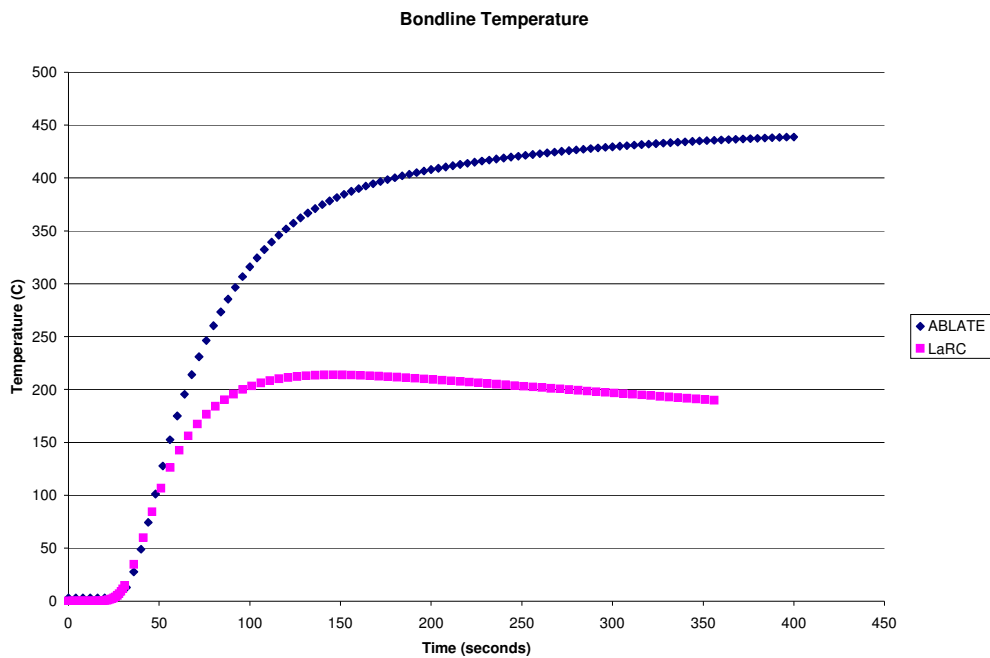
Figure 9: Bondline temperature vs. time

If the parameters, heat of ablation and temperature of ablation, are adjusted to match the bondline temperature results from CMA, then the stagnation-point surface recession

results will no longer match. It should be noted that the adjustments made are done manually and not using an optimizer. The addition of an optimizer can automate the adjustment of the two parameters within ABLATE to most closely reproduce the results from CMA. However, the optimizer option was not considered in the scope of this report.

With CMA's results correlated using ABLATE, the next step is to integrate it with the parametric geometry environment. As mentioned in the implementation section, the geometry will be created using Thermal Desktop. Figure 10 shows a generic entry vehicle defined by variables. In order to demonstrate the flexibility of the parametric model, different entry vehicles were modeled. Specifically, the Viking, Pathfinder, and Stardust entry systems were chosen. Figure 11 shows a comparison of the schematic of the entry system and the parametric model. While the parametric model is not a 100% representation of the schematic, it captures the essential features of the entry system. Furthermore, during preliminary design, these features would be sufficient for ablation analysis.
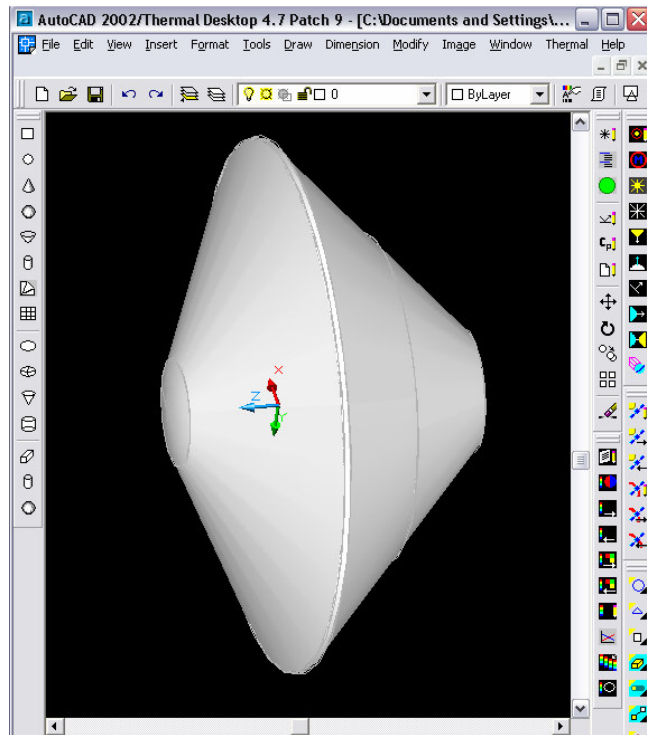
Figure 10: Parametrically defined generic entry vehicle
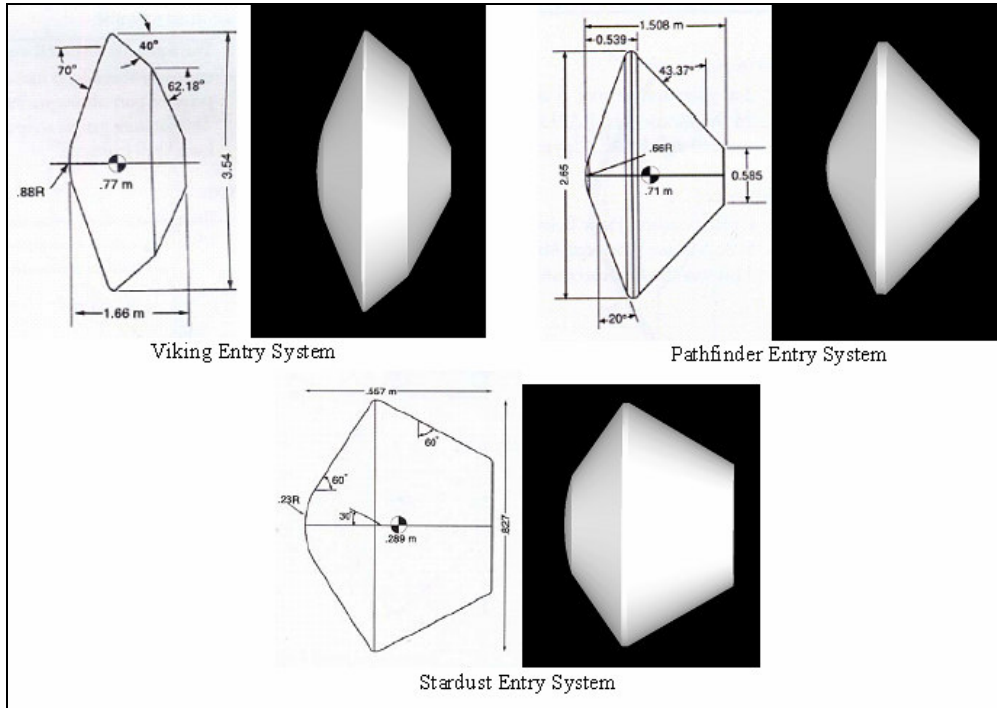
Figure 11: 3 entry systems both in schematic and parametric model

The actual integration of the ABLATE tool and the parametric geometry environment did not involve much additional work. At the time this idea of integration was proposed, C&R Technologies, the creator of Thermal Desktop and SINDA, released version Thermal Desktop 4.7. This version couples the ABLATE tool within the CAD environment of Thermal Desktop. Figure 12, is an example of the integration of the ABLATE tool within the parametric geometry environment.
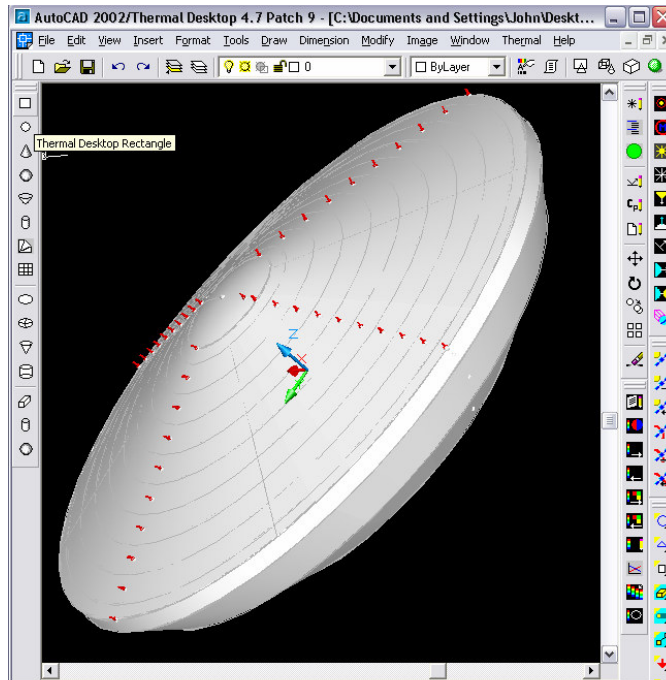
Figure 12: Thermal Desktop V4.7 with ABLATE tool integrated

Within the parametric environment, the heat load was specified for the forebody and the ABLATE tool was run on the geometry. The ablative material properties can also be specified in Thermal Desktop. The same EEV example was successfully run with similar results.

3.5 Summary

The thermal task set out to investigate a quick-sizing ablation tool: ABLATE. The sample case used was the Earth Entry Vehicle that uses carbon phenolic as its ablative material. Using results from a validated software, CMA, ABLATE was correlated. Initially, correlation was difficult because of way ABLATE approximates ablative processes. Specific parameters that ABLATE uses had to be acquired by attempting to reproduce CMA's results for surface recession and bondline temperatures. In the end, the method of correlation doesn't prove the validity of ABLATE. Instead, some doubts arose in the parameters ABLATE uses to approximate ablation characteristics. However, additional studies could show if ABLATE indeed is a sufficiently accurate tool for preliminary ablative material design.

3.5.1 Achievements

Investigating how ABLATE approximates ablation was one of the primary goals for the thermal task. Understanding the parameters and how they are used within ABLATE would shed light on the usefulness of the tool. A full case was successfully run using ABLATE, both in SINDA and the parametric geometry environment (Thermal Desktop). Furthermore, the parametric geometry environment was shown to be a flexible model

by modeling different entry systems with different geometries such as Stardust, Pathfinder, and Viking. Finally, both the ABLATE tool and the parametric geometry environment were linked together.

3.5.2 Lessons Learned

Several important lessons were learned during the exercise of modeling the EEV using the ABLATE tool. The first lesson was regarding the ablation parameter, heat of ablation. Heat of ablation is a data correlation parameter that can be used only for steady-state ablation and not for transient cases. Since ABLATE uses this parameter, its ablation approximation is flawed. Rather than abandoning the ABLATE tool altogether, this flaw was used as an opportunity to correlate the data from CMA with ABLATE's. Therefore, the results were used to back-solve what the heat of ablation parameter value should be. Future studies would show how to better approximate heat of ablation or whether to use it at all.

Another invaluable lesson was learned when linking the parametric geometry environment with the ABLATE tool. When the geometry was altered, there wasn't any change to the results from the ABLATE tool such as increased ablative material recession or a different bondline temperature profile. Looking further into the ABLATE code, the reason why this occurred was discovered. The heating loads for the EEV case were entered as an input file rather than being calculated from the geometry of the entry vehicle. Thus, an altered geometry would have no direct impact on the results from the ABLATE tool.

3.5.3 Recommendations for Future Work

Currently, the correlation of the data is done by manually changing the ABLATE parameters. However, as mentioned earlier in the report, an automated process can significantly reduce the time necessary to correlate data. Furthermore, using an optimizer to reduce the error in the results from the two tools will improve ABLATE's efficiency. The optimizer will attempt to reduce the error by parametrically changing the heat of ablation and temperature of ablation parameters. This will allow ABLATE to be used to correlate other entry cases.

The above recommendation leads to the second recommendation. So far, ABLATE has been used only to correlate data for the EEV. One way of gauging ABLATE's usefulness would be to correlate other missions. Missions similar to the EEV as well as drastically different would give valuable insight about how accurate or consistent ABLATE's results are. For example, the Galileo entry vehicle (Jupiter) and the Mars microprobes would be two missions that would be beneficial to model. The Galileo entry vehicle faced high radiative heating as it entered Jupiter's atmosphere. The Mars microprobes were a lot smaller in dimension compared to other entry systems and would therefore have a unique heat load and therefore unique ablative characteristics. Granted these to cases at either end of the spectrum, they would nonetheless demonstrate whether ABLATE's range if it indeed does span the spectrum.

4 Aerodynamics Task

4.1 Introduction

An understanding of the aerodynamics of a planetary entry vehicle is essential for a successful mission. The aerodynamics contribute to the analysis of the vehicle as soon as it enters into the planet's atmosphere continuing until it lands on the surface. This task's goal is to create a low speed aerodynamic model for an entry vehicle that can be utilized as a quick design tool in the preliminary phases of design. The model is concentrated near parachute deployment, which is in the range of Mach 1.25 to 2.5. The tool will use high resolution data from a computationally intensive tool and create a quick-look model for assessing key aerodynamic characteristics such as lift coefficient (C_L), drag coefficient (C_D), pitching moment coefficient (C_{My}), and lift over drag (L/D) as a function of Mach number, angle of attack, and center of gravity location.

An increase in the knowledge of how the entry vehicle's aerodynamics behave early in the design process can significantly increase the body's landed accuracy. A vehicle that uses lift to maneuver in the atmosphere will have a smaller landing ellipse than one that does not. An example of how the dispersion size can be improved using lift is shown in Figure 13.
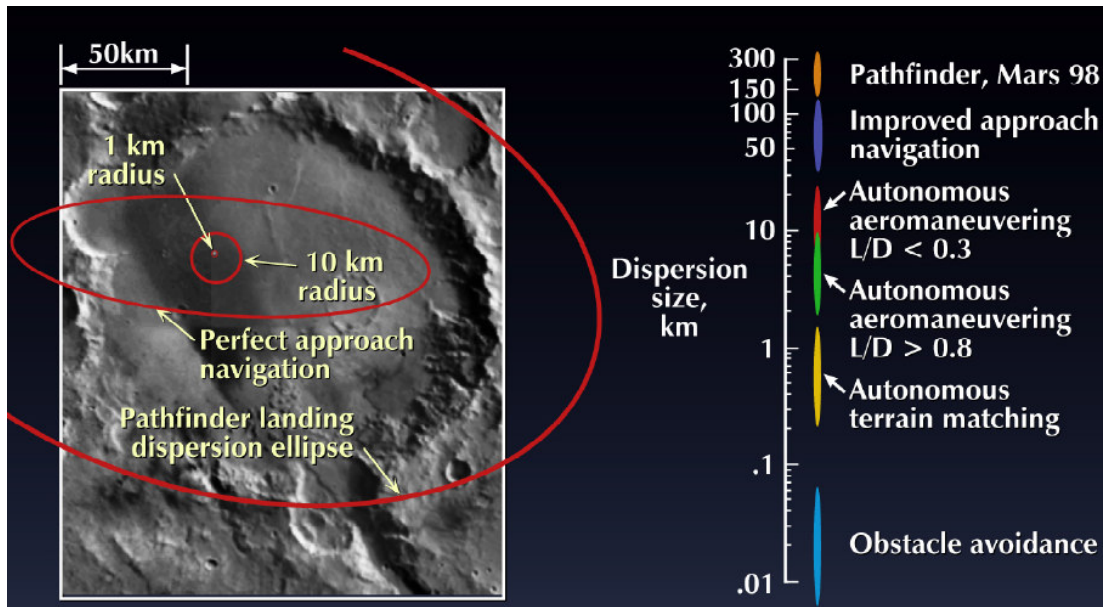
Figure 13: Landing accuracy based upon type of aeromaneuvering used[12]

As L/D is increased, the dispersion size greatly decreases from approximately a 50 km radius using no lift to approximately a tenth of that radius using a L/D greater than 0.8. Because current entry vehicles do not have control surfaces, they must use a shift in center of gravity to obtain a trim condition which will give an angle of attack that results in a certain amount of lift. This tactic is limited in the amount of lift it can generate; therefore this task will study L/D's in the range of about 0.1 to 0.3. The figure illustrates that this range of L/D can decrease the landing ellipse radius to 10 km or less.

The aerodynamics task aspires to prove that this method can be applied to any project where it is necessary to take data from a computationally intensive program which may take weeks or months to run, and create a quick-look model using the program's output. While this task is specific to a Mars entry vehicle, the steps applied to create the quick-look design tool can be applied to other projects to create a similar model.

4.2 Approach

The response surface methodology described in the Metamodel section of the report is used for the aerodynamics task. Aerodynamic data obtained from a CFD code is utilized to create response surface equations which designers can use in the preliminary design phase. These equations will give engineers ballpark estimates for angle of attack and Mach number needed to achieve a certain amount of lift. The lift can be used for

aeromaneuvering which will increase the landed accuracy. The equations will help approximate the landing ellipse size.

The RSEs, as explained in the Metamodel Methodology section, have a tradeoff between accuracy and speed. The designers must realize that in order for increased speed, they will be giving up some on accuracy. Early in the design process, though, this trade off is beneficial because many different designs and trade-offs can be analyzed, instead of just a few.

4.3 Implementation

A computational fluid dynamics (CFD) code, Computational Fluids Laboratory 3-Dimensional flow solver (CFL3D), is used to obtain values of C_L, C_D, C_{My}, and L/D over a range of various input parameters shown in Table 2. CFL3D is a Reynolds-Averaged thin-layer Navier-Stokes flow solver for structured grids. In this case, CFL3D uses a Mars Exploration Rover (MER) entry vehicle as its reference grid. A sample of the input file for CFL3D is illustrated in Figure 14.

Table 2: The design variables and their ranges

Design Variables	Range
Mach Number, M	*1.25-2.5*
Angle of attack, α	*0-12 degrees*
Moment Center in Z-direction, Z_{mc}	*0-0.2*
Moment Center in X-direction, X_{mc}	0.405-0.455

```
I/o files
mars03_regrid_flip.unf_dp
mars03_p3d.g
mars03_p3d.q
mars03.out
mars03.res
mars03.turres
mars03.blomax
mars03.out15
mars03.prout
mars03.out20
mars03.ovrlp
mars03.patch
mars03.restart
>
ibin 0
iblnk 0
epsa_r 0.30
<
   Mars03
      xmach     alpha      beta   reue.mil   tinf.dr     ialph     ihist
      1.5000    -5.000       0.0     6.000     460.0         0         0
       sref      cref      bref       xmc       ymc       zmc
     5.52000   1.00000    1.5000   0.40500      0.00      0.00
         dt     irest    iflagts      fmax     iunst    cfltau
      -0.05         0      1000      20.0         0      10.0
      ngrid    nplot3d    nprint    nwrest      ichk       i2d    ntstep
        -14       +14         0       500         0         0         1
```

Figure 14: Screenshot of a portion of the input file for CFL3D

CFL3D is a computationally intensive program, which can take up to one hour to run a single case. In order to expedite the process of obtaining data points for the model, a script was created by Dr. Robert Weston of NASA Langley that utilizes a user created table of eight cases for the values of the input parameters. Each case has different values for the design variables, and the script inputs each case into a separate run of CFL3D. Each case is run on a different computer, which allows for eight to be run in one hour, as opposed to one. This process is utilized to populate the design space over the range of the design variables.

Once enough points are generated, they are copied over to JMP, the statistical software tool described in the Metamodel Methodology section. JMP is used to create a best fit model, using the CFL3D data to generate response surface equations, where C_L, C_D, C_{My}, and L/D are the responses and M, α, etc. are they design variables. JMP uses least squares regression to obtain its model, which minimizes the sum of the squares of the differences between the data points (actual data from CFL3D) and its best fit-model (predicted data from JMP best-fit line). In order to increase the accuracy of the model, a few higher order terms (3rd order) were added into the response surface equations. Adding the higher order terms allowed the model to account for some of the more irregular trends.

JMP has tools built in to determine and asses the accuracy of the model, and if necessary, improve the response surface equations. The residual by predicted plot for the C_L response is shown in Figure 15 and the actual by predicted plot is illustrated in Figure 16. These tools help analyze data to verify the accuracy and validity of the responses.

Once the model is determined to be a good fit, the parameter estimates for each response are copied from JMP to Microsoft Excel. The parameter estimates are terms which are used to multiply their respective design variables or combination of design variables to obtain an estimate for the response. These estimates are essentially the constant coefficients used in a equation which multiply the variables in order to calculate the "answer", which in this case is either C_L, C_D, C_{My}, or L/D. The terms for the C_L equation are displayed in Table 3 below.
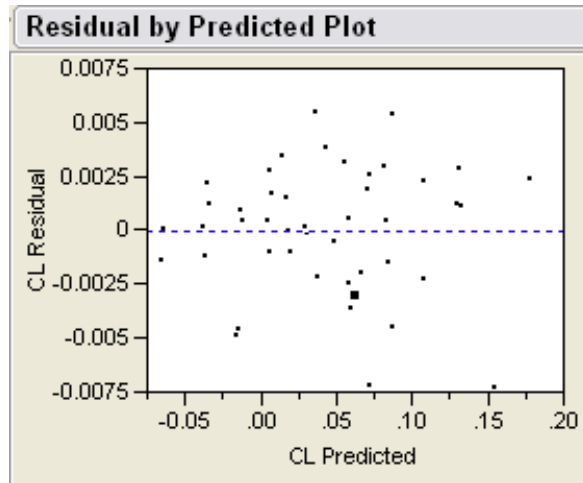
Figure 15: Residual by Predicted plot for C_L
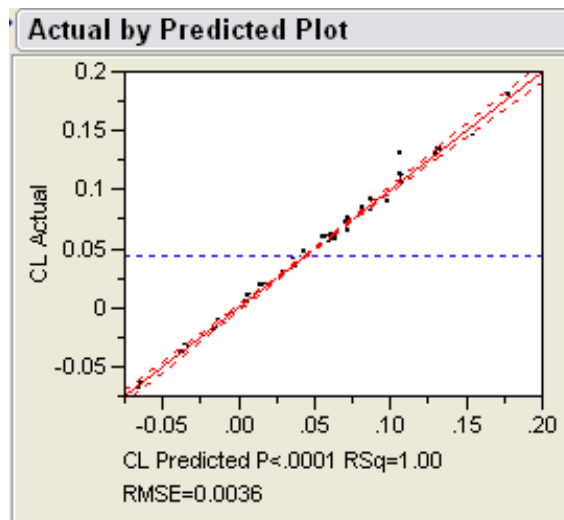
Figure 16: Actual by Predicted Plot for C_L

Table 3: Table of parameter estimates for CL response

Term	Estimate
Intercept	0.7435206
M	-0.914144
AoA	-0.004876
Zmc	0.4476296
M*M	0.3626492
AoA*M	-0.00984
AoA*AoA	0.0065049
Zmc*M	-0.471693
Zmc*AoA	-0.050858
Zmc*Zmc	0
M*M*M	-0.053791
AoA*M*M	0.0076693
AoA*AoA*M	-0.000884
AoA*AoA*AoA	-0.000328
Zmc*M*M	0.1202715
Zmc*AoA*M	0.0217143
Zmc*AoA*AoA	0.0039923
Zmc*Zmc*M	0
Zmc*Zmc*AoA	0
Zmc*Zmc*Zmc	0

Microsoft Excel allows for efficient calculation of the response values. Excel takes values for the design variables from Table 2, and using the parameter estimates, calculates and outputs approximations for the responses. The advantage of using a response surface equation is that the design variables can take values which were not used as design points in CFL3D. This model allows for calculations over the whole range of the design space.

4.4 Demonstration

The aerodynamics tool is straightforward to use. An Excel spreadsheet contains all the necessary equations and parameters and a section for the inputs and outputs. The calculations run in the background on a separate spreadsheet. The input and output

Input Parameters		Allowable Range	Input Value
Mach Number	M	1.25-2.25	2.2
Angle of Attack	α (degrees)	0-8	7.5
Moment center in Z direction	Zmc	0-0.2	0
Moment center in X direction	Xmc	0.405-0.455	0
Aerodynamic Terms		**Predicted Value**	
Lift Coefficient	CL	0.1125	
Drag Coefficient	CD	0.2154	
Pitching Moment Coefficient	Cmy	-0.004971	
Lift over Drag	L/D	0.5610	

Figure 17: Screenshot of the input and output section of the aero

section is shown in Figure 17. The input box shows the design variables and their allowable range. An input value can be any number within the allowable range, even if

the value was not an original design point. The output box displays the predicted values for the terms of interest. The response surface equations running in the background use the input values and the parameter estimates to output the predicted values.

An example run of the aerodynamic tool can also be seen in Figure 17. Values for Mach number and angle of attack were set at 2.2 and 7.5 degrees, respectively. The moment centers were unchanged from their default value. The tool's runtime is just as long as it takes to type in the input values. The tool instantaneously outputs the predicted values for C_L, C_D, C_{My}, and L/D. This case has a predicted lift over drag of 0.5610, which Figure 13 shows will help obtain a dispersion size of 10 km or less.

4.5 Summary

4.5.1 Achievements

A first-order aerodynamics tool was created that can be used in preliminary design to analyze the aerodynamics of a Mars entry vehicle. The tool takes data points generated from a CFD code and uses these points to create response surface equations. The equations have Mach number, angle of attack, and center of mass locations as the inputs and they output estimates for the vehicle's aerodynamic coefficients C_L, C_D, C_{My}, and L/D. The tool allows for quick estimates of aerodynamic parameters in the early stages of design.

4.5.2 Lessons Learned

This task showed that any future projects that require data analysis from slow programs but do not have the time to run them during the design phase can utilize the procedure described in this report. The data points can be gathered over a range that will encompass all the possible design cases, a couple weeks prior to the commencement of the design phase. The metamodel created from the cases can then be used as a quick design tool in the design phase.

An important detail to remember about RSEs is that they give up some accuracy for speed. The designer who decides to use RSEs for a quick reference must recognize the fact that they can only use the RSEs as an estimate. This characteristic of metamodels makes them a perfect tool for early design phases.

4.5.3 Recommendations for Future Work

The aerodynamics task, while completing its goals, has other work which could be added to the current accomplishments. Future work on the tool could include:

◇ Run cases with morphing grid and add geometric variables into RSEs

◇ Expansion of the ranges of the design variables, specifically Mach number and angle of attack

◇ Acquire a more efficient grid

◇ Acquire prototype grids of shapes engineers are considering for new Mars missions

◇ Validate the tool with actual data from MER

◇ Run more cases to obtain additional data points

◇ Study c.g. change needed for trim

5 Risk Task

5.1 Introduction

The recent success of the Mars Exploration Rover missions received much attention and deserved praise. The entry, descent, and landing airbag-assisted design safely landed both the Spirit and Opportunity rovers on Mars in January 2004. Entry, descent, and landing (EDL), however is far from routine for interplanetary probes or Earth return vehicles. There have been several high profile failures including the 1999 Mars Polar Lander, the British led Beagle 2 lander in December of 2003, and the recent crash landing of the Genesis solar wind collecting spacecraft in September 2004.

The risk task responds to a need for an early assessment of EDL mission risk in spacecraft design. In a general sense, spacecraft design involves making design choices that trade risk, capability, and resources to arrive at an optimal solution given certain objectives. Knowledge of failures and uncertainty provides information on which risks can be quantified. Figure 18 graphically shows this process.
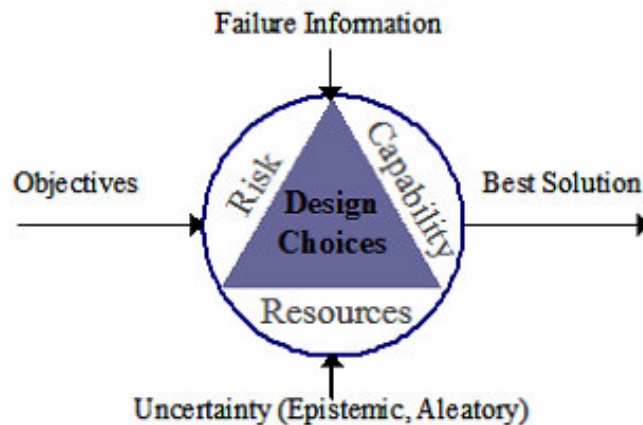
Figure 18: Spacecraft Design Process

Integration of risk and design models benefits the EDL conceptual space systems design process as implemented by NASA JPL Team X and assisted by NASA Langley. Enabling early assessment of mission risk will allow Team X designers to perform trades between risk and design performance during the initial design space exploration. Furthermore, the methodology developed may have application to other disciplines, or the risk characterization process in general, within Team X. An EDL risk evaluation methodology and tool could serve to facilitate communication and as a repository for Langley EDL knowledge. The Langley ECS risk competencies have potential to benefit

from the methodology in much the same way as JPL Team X, by exposure to a novel approach to risk characterization.

The specific goals of the risk task were to develop the following:

1) Generic EDL risk architecture

2) Road map for EDL mission design and a capability for evaluating options

3) Methodology to facilitate tracking and visualization of EDL technical risks

There is a large degree of uncertainty for many aspects of EDL due to limited experience and knowledge, especially for planets other than Earth. This uncertainty arises from environmental sources such as the characteristics of the atmosphere, and from errors in modeling and measurement. Designing to reduce these uncertainties can be just as important as preventing hardware failures from occurring. Thus, a key aspect of the methodology development was the need to account for risks due to both epistemic and aleatory uncertainties. EDL designs also often feature new technologies. Since these technologies can not be predicted, the methodology needed to be capable of assessing new technologies. Finally, the suggested methodology needed to have sufficient flexibility to permit future expansion.

The methodology resulting from the risk task involves the use of Event Sequence Diagrams (ESDs) and Fault Trees (FTs) together with the Defect Detection and Prevention risk tool. The ESDs and FTs depict the risk architectures and organize objectives, risks, and mitigations for creating the DDP model. The DDP risk tool demonstrates a possible means of trading risk, capabilities, and resources during the design phase.

5.2 Approach

The approach to meeting the research goals consisted of three major phases: research, architecture organization, and risk tool setup.
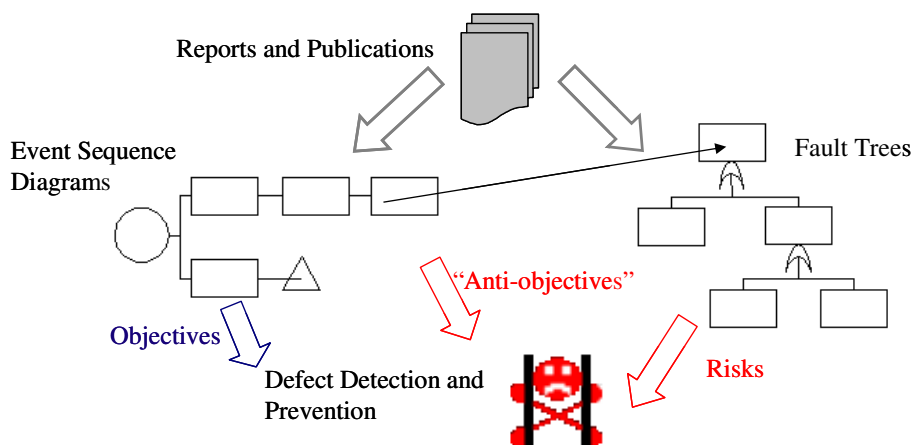

Figure 19: Diagram of Approach

5.2.1 Research Phase

Research was conducted to become familiar with EDL missions, designs, and technologies. Scholarly journals were the primary source of information. A wealth of information was found in Reports published by the American Institute of Aeronautics and Astronautics, Institute of Electrical and Electronics Engineers, Academy of Applied Sciences, International Astronautic Federation, etc. In addition, the researcher attended a short course on Planetary Entry, Descent, and Landing presented by Dr. Robert Braun of Georgia Tech. Textbooks served as a third source of information.

5.2.2 Architecture Organization Phase

In the architecture organization phase, Event Sequence Diagrams describing possible EDL architectures were created from the various EDL mission profiles discovered in the research step. The events in the ESDs describe the events that must occur for a successful EDL mission. The events also delineate many of the design choices as there may be more than one design solution that can accomplish the sequence event. Fault Trees were developed for many of the events in the ESDs, again using information from the prior research. The fault trees include hardware failures, software failures, and uncertainties in modeling or measurement that could cause the event to not occur.

5.2.3 Risk Tool Setup Phase

In the risk tool setup phase, the ESDs and FTs are captured within the Defect, Detection, and Prevention risk analysis software. A DDP model of EDL mission choices was created such that a user can make EDL design trades based on capability, risk, and cost. The DDP model allows for the user to select events necessary for mission success and consider possible design solutions for those events.

5.2.3.1 DDP

The Defect Detection and Prevention software program is a risk management tool developed principally by Dr. Steven Cornford and Dr. Martin Feather of the NASA Jet Propulsion Laboratory. DDP was chosen as the risk tool for the following reasons:

- ◇ Well developed and readily available
- ◇ Accessibility of support
- ◇ Ability to accept multiple types of quantification data
- ◇ Built in risk fault tree capability
- ◇ Additional capabilities, functions, and customization

In addition to these reasons, the risks generated for DDP can be relatively easily exported for import into the RAP risk tool used by the JPL Team X conceptual design team. Other advantages of DDP are discussed in the sections below on implementation.

The standard DDP process, depicted in Figure 20, involves defining objectives, risks, and mitigations; scoring the risks against the objectives and the mitigations against the

risks; and using the risk balance and objective attainment functions to find the best design solution.

5.2.3.2 Translating ESD and FT to DDP

The DDP objectives can be thought of as the successful outcomes of the ESDs. For example, the positive outcome of successful completion of all events in the sequence becomes the objective "complete EDL mission" within DDP. The ESD events are translated into DDP anti-objectives, which are the top level risks. For example, the event "supersonic parachute deploy" is translated into a top level risk in DDP of "failure during supersonic deceleration." The fault tree events become the risks within DDP. In this way, the same hierarchical structure of FT underlying ESD event is maintained in the DDP risk tree with risks underlying anti-objectives.

5.3 Implementation

While the standard DDP process provides a general roadmap, there is a great deal of flexibility available in creating a DDP model. This flexibility is advantageous and powerful, but necessitates some rules to maintain consistency in setting up and using DDP. These rules were applied at the objective, risk, and mitigation level. Mitigations were further broken down into Design Switch Mitigations and Improvement Mitigations.
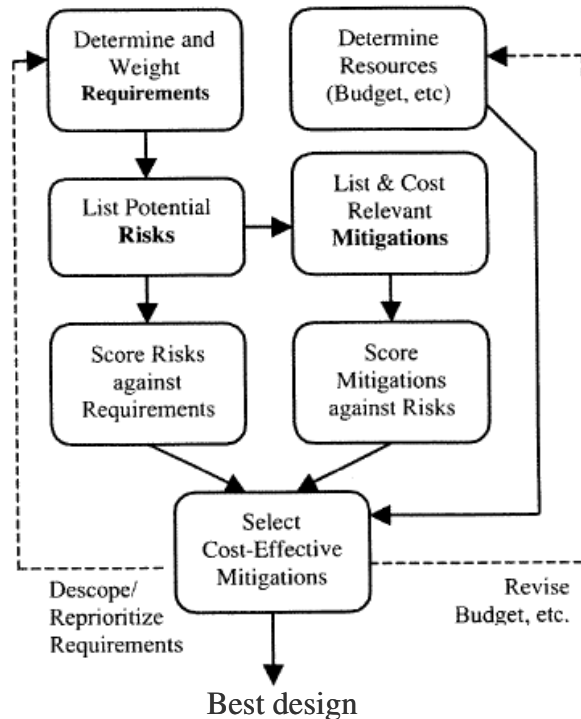
Figure 20: Standard DDP Process [13]

5.3.1 Objectives

The objectives are intentionally kept broad and generic. This allows for evaluation of the various design choices against a common metric. For example, there may be a scenario where a lander and a glider are being considered for a particular mission. A lander and a glider may have some sequence events in common, but likely have several significantly different specific events that must occur for mission success. The objective "complete EDL mission" is sufficiently broad to serve as an objective against which both design possibilities can be considered.

Three types of objectives were identified: sequence, science, and engineering. Sequence Objectives are those related to completion of events in the mission sequence. Science Objectives refer to the ability to perform the desired science investigation as effected by the EDL design. Landed accuracy is an example of a Science Objective. One can easily foresee a design scenario where the science requirements call for a pinpoint landing to investigate a previously identified location of scientific interest. Engineering Objectives refer to the collection of data to improve future missions, or proof of concept demonstrations conducted in addition to, or as part of, the EDL mission. Accelerometer or atmospheric density measurements are examples of collected data that might satisfy Engineering Objectives.

When scoring the risks against the objectives, the Science and Engineering Objectives are considered given that the Sequence Objectives have been completed. This is because the Science and Engineering Objectives are assumed to be inconsequential if a failure prevents the sequence from being completed. While in actual operations, engineering data might be useful for reconstructing why a failure occurred, this assumption is valid at the design stage. Certainly engineers do not design spacecraft expecting them to fail.

5.3.2 Risks

Risks in the DDP model seek to capture the risks associated with the selection of various design solutions. These design solutions may be historically proven or pioneering inventions. Functional decomposition stops at the component level. Any uncertainties in modeling or measurement considered also have effect at the component level or higher. Quantification at the parts level is unnecessary given the fidelity of design trades at the conceptual design level. Consideration of parts would furthermore expand the number of risks considerably.

In scoring the impact of the risks on the objectives, the standard DDP approach is taken. If the risk occurs, by how much will it contribute to loss of the objectives? This could also be thought of as the percentage of objective lost due to the risk occurring. The impacts are scored against the objectives at the top level of the tree for the Sequence Objectives. Recall that the top level risks are the anti-objectives, which are the events that must occur to complete the mission. Thus, the impact of the top level risks on the objective is equal to one in most cases. If the top level risk occurs, 100 percent of the objective will be lost and the mission will not be a success. The impacts of risks on other objectives such as Engineering and Science, however, are scored at the subrisk (leaf) level. Recall that the Engineering and Science Objectives assume that the sequence has been completed successfully. If the sequence has been completed, all of the top level anti-objective risks have been met. However, a subrisk could have occurred causing a degraded level of operation. For example, a lander may satisfy the sequence objectives by successfully landing on the surface, but error in parachute measurements prevent it from achieving the pinpoint landing that was desired for science reasons.

DDP affords excellent flexibility for risks because the impact of the risks is considered as a loss of the objectives. Risks can describe hardware failures, software failures, procedural mistakes, and epistemic and aleatory uncertainties. Furthermore, this flexibility allows for risks to be considered independent of time. Risks that describe negative occurrences during design, testing, operations, etc. can all be considered concurrently. Each has some measurable undesirable consequence that contributes to loss of the objectives, but it does not matter when the risk actually occurs.

5.3.3 Design Switch Mitigations

Design Switch Mitigations, or simply Design Switches, are used to activate and deactivate various risks. This is necessary because most risks are associated with the use of a particular design solution. For example, when the mitigation "use Viking heritage

parachute" is selected, the risks associated with using a Viking heritage parachute are activated.

Activation of the risks is accomplished by setting the risk a-priori likelihood equal to zero and scoring the mitigations against the risks negatively. Making the risk a-priori likelihood equal to zero means that the risk has zero probability of occurring. A risk can be made more likely by a mitigation scored negatively. In this situation, the mitigation is inducing a risk to occur. Design Switches induce a previously zero a-priori likelihood risk to some non-zero likelihood, thus activating the risk. This use of Design Switch Mitigations is illustrated in Figure 21 below. When mitigation "Use Design Choice A" is checked, the previously zero (a-priori) likelihoods of Risk A1 and A2 become non-zero because the mitigation of those risks has been scored negatively.
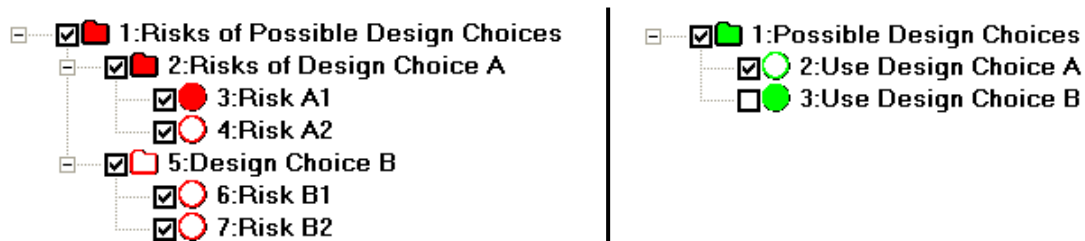
Figure 21: Design Switch Mitigations

The use of Design Switches provides the ability to make design trades. The design trades are accomplished by selecting design options at the mitigation level. When scoring the Design Switch Mitigations against the risks, the scored effect is the likelihood of each risk occurring given the selection of each design choice.

5.3.4 Improvement Mitigations

Improvement Mitigations capture actions taken to improve upon a portion of the design. The risks associated with historically proven design solutions and pioneering inventions may be mitigated somewhat by improvements. These mitigations are scored against the risks using the standard DDP approach. The effect of the mitigation on the risk is positive and reflects the probability of preventing or detecting the risk. By how much (percent) does the mitigation reduce the risk if it is employed?

The traditional DDP PACTS best describe Improvement Mitigations. PACTS are "Preventative measures (e.g. design rules, material and parts selection, architecture, redundancy), Analyses (e.g. structural, optical, chemical, electrical performance, FMECAs and other reliability analyses), process Controls (e.g. inspections, coupon sampling, standard procedures and processes), and Tests (e.g. functional, environmental, stress screening)" [14]. It is important to note that redundancy in components is considered an Improvement Mitigation. This allows the designer to

consider the reduction in risk gained from a redundant system. In addition, Improvement Mitigations include enhancement to historically proven design through new models or reduced uncertainty. This is important as it allows for consideration of how a design is affected by reducing risk through decreased uncertainty.

5.3.5 Design Trades and Optimization

After the objectives, risks, and mitigations are entered and scored, design trades can be conducted by selecting mitigations. The Design Switch Mitigations allow for selection of design solutions. A design can then be improved upon by adding improvement mitigations. Optimization of the design is possible through the DDP built-in simulated annealing optimizer since all design trades are accomplished at the mitigation level. The optimizer shows risk versus cost for the combination of mitigations available. The best design depends on the level of acceptable risk and cost, but in general better designs are characterized by lower risk for their cost.

5.3.6 Possible Quantification Sources

While population of a DDP model by quantifying the objectives, risks, and mitigations with real data was not within the scope of this project, several potential quantification sources exist and are worth mentioning. Some possible sources include:

◇ Historical data

◇ Expert opinion

◇ Generic cases run in analysis tools

◇ Back of the envelope calculations

◇ High fidelity analyses

Each of these sources has advantages and disadvantages. Different sources may be more appropriate than others for different risks, and information unavailability may necessitate the use of a particular source. The output of any of these sources, regardless of fidelity, can be input into DDP. The capability to combine data from multiple sources is an excellent quality of DDP.

5.4 Demonstration

The developed methodology is demonstrated through two typical EDL sequence events; navigation to the planetary interface and descent on supersonic parachute. For simplicity, these events will be referred to as navigation and supersonic deceleration.

5.4.1 DDP Demonstration Model

A portion of the EDL ESD is shown in Figure 22. The sequence progresses from left to right and the navigation events appear to the far left of the diagram. Events stacked vertically indicate design choices. For example, the design may use DSN Doppler and Ranging to navigate to the planet or Optical Navigation. In some cases, like in this

example, both choices can be used together. A portion of the fault tree for supersonic parachute is shown in Figure 24. Note that the fault tree contains hardware failures, software failures, modeling uncertainty, and environmental uncertainty.

The standard DDP process as depicted in Figure 20 was followed according to the previously defined rules to create the DDP demonstration model. Figure 22 below shows the objectives and their weights. Note that there is a single Sequence Objective, a Science Objective with three sub-objectives of varying degree, and a single broad Engineering Objective.
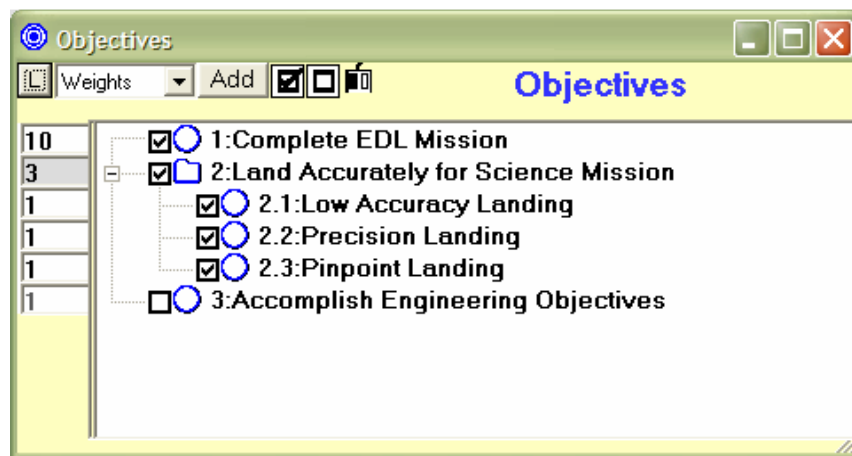
Figure 22: Objectives for DDP Demonstration Model

Trajectory Phase | Aeroassist Phase | Atmospheric Entry Phase
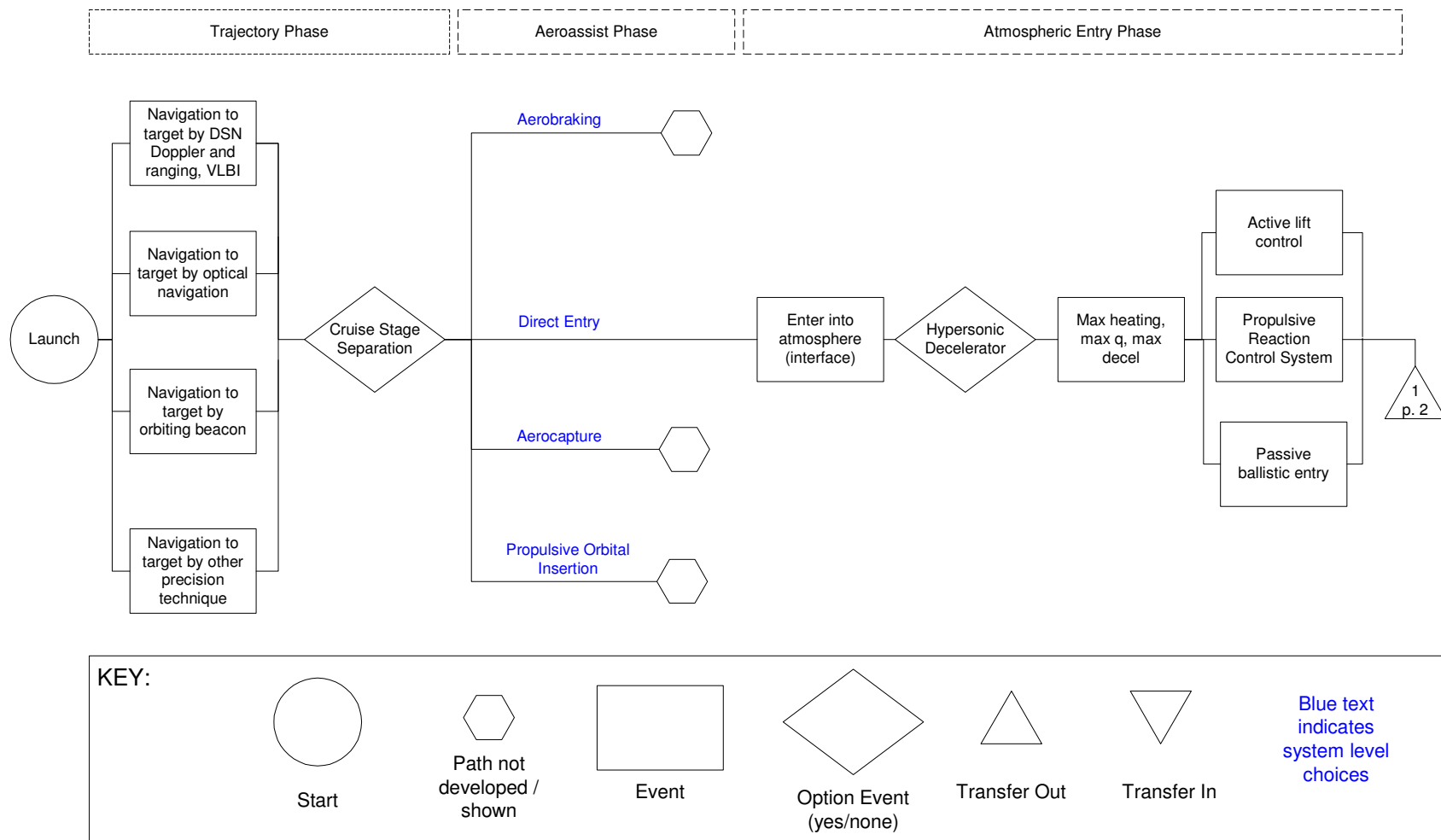
Figure 23: Portion of Event Sequence Diagram for Demonstration
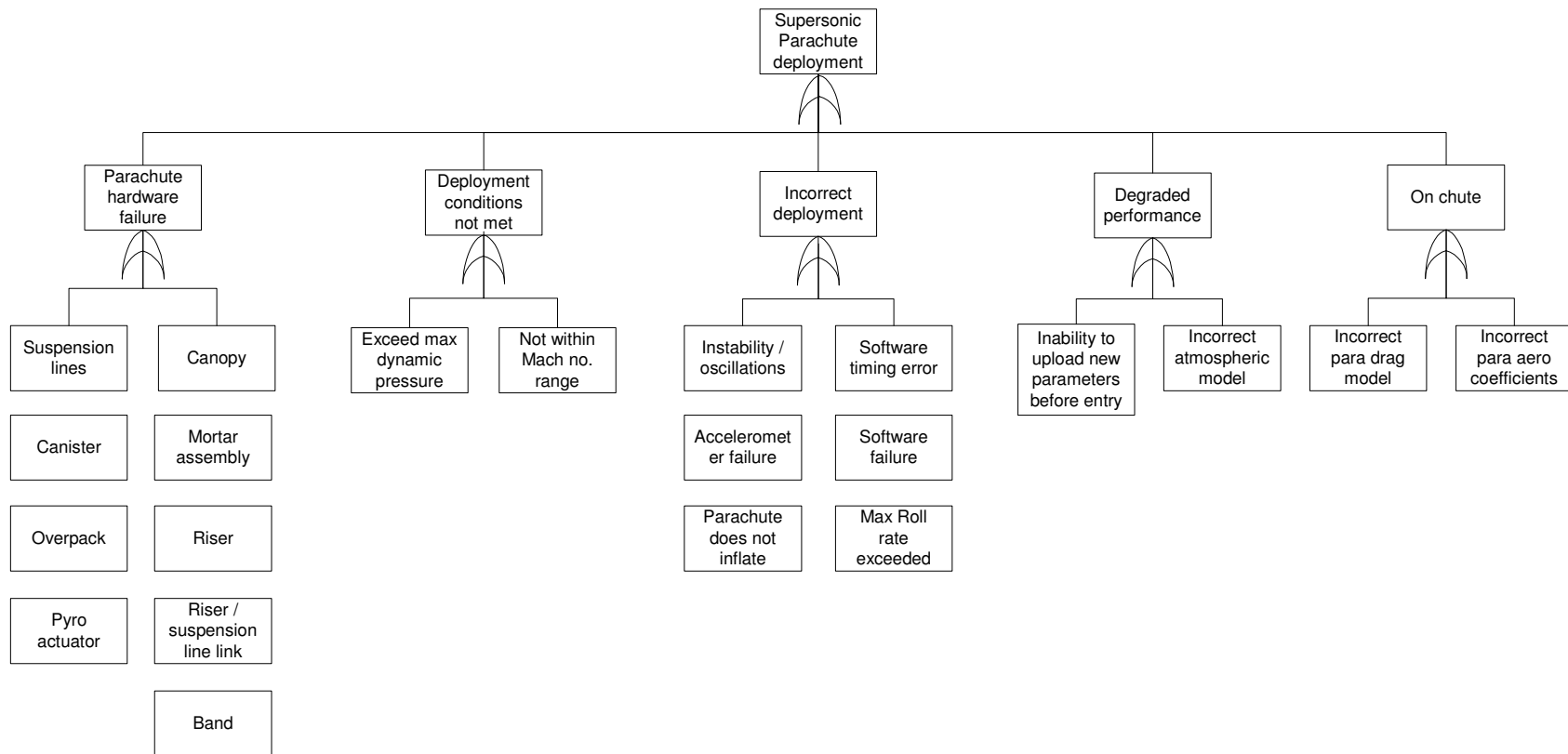
Figure 24: Portion of Supersonic Deceleration Fault Tree for Demonstration

A condensed risk tree is shown in Figure 25. Risks 1.1, "Inability to Navigate to Planet," and 5.1, "Inability to Descend," are examples of anti-objectives. Supersonic deceleration, risk 5.1.4, is a sub-tree to terminal descent phase. The expanded supersonic deceleration tree is shown in Figure 26 and is comparable to the fault tree shown in Figure 24.
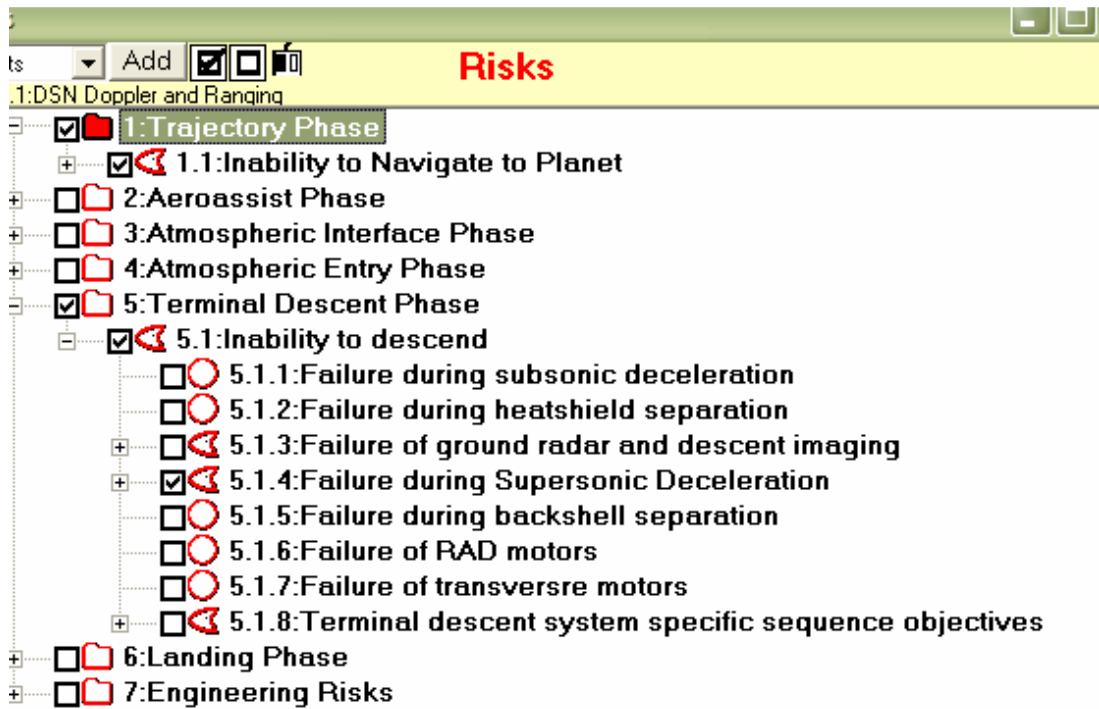
Figure 25: Condensed Risks of DDP Demonstration Model
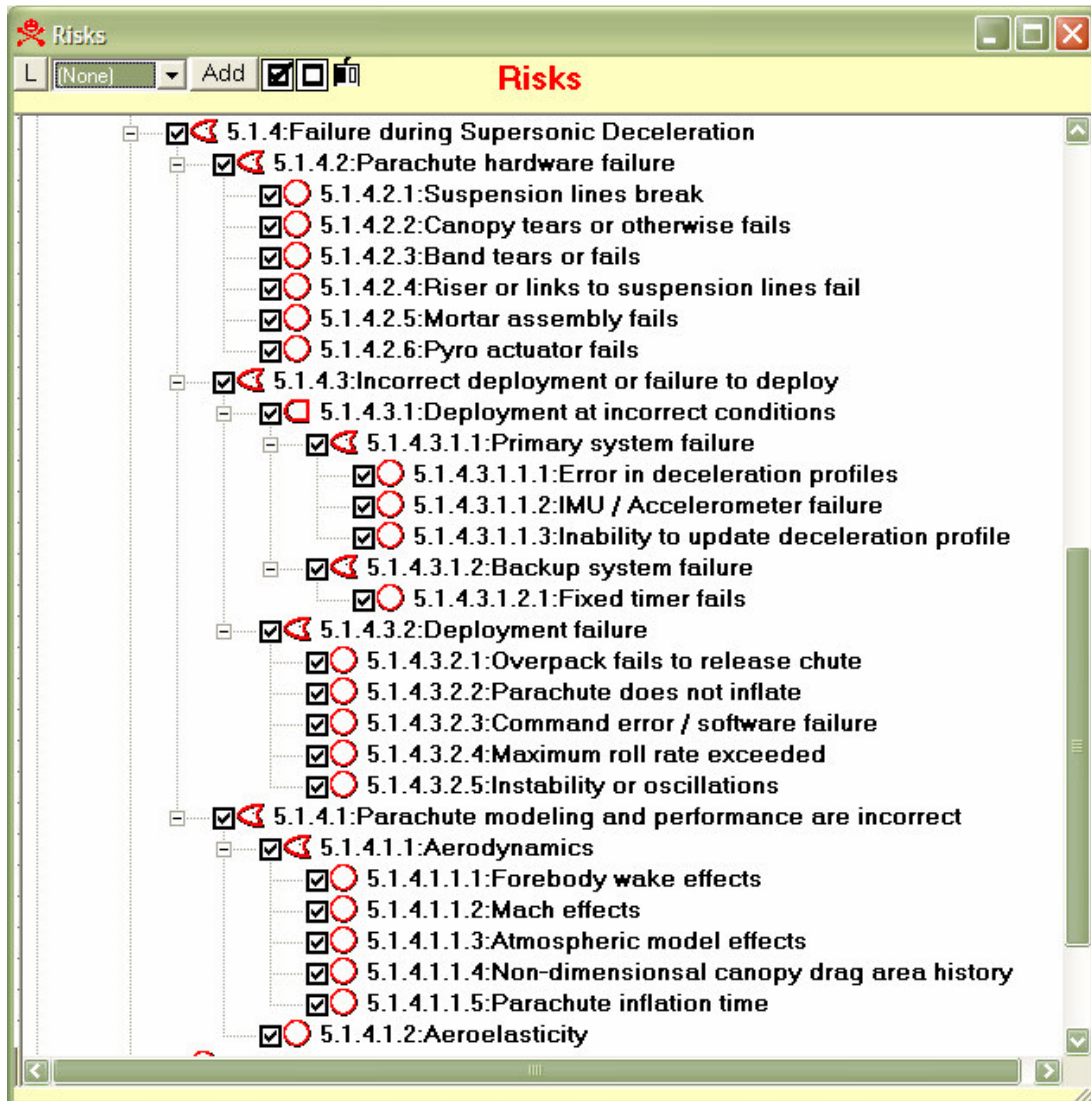
Figure 26: Supersonic Deceleration Risks of DDP Demonstration Model

The mitigations tree shown in Figure 27 consists of the navigation system and supersonic deceleration mitigations considered for the demonstration. The navigation design choices are examples of Design Switch Mitigations while the navigation improvements are examples of Improvement Mitigations.
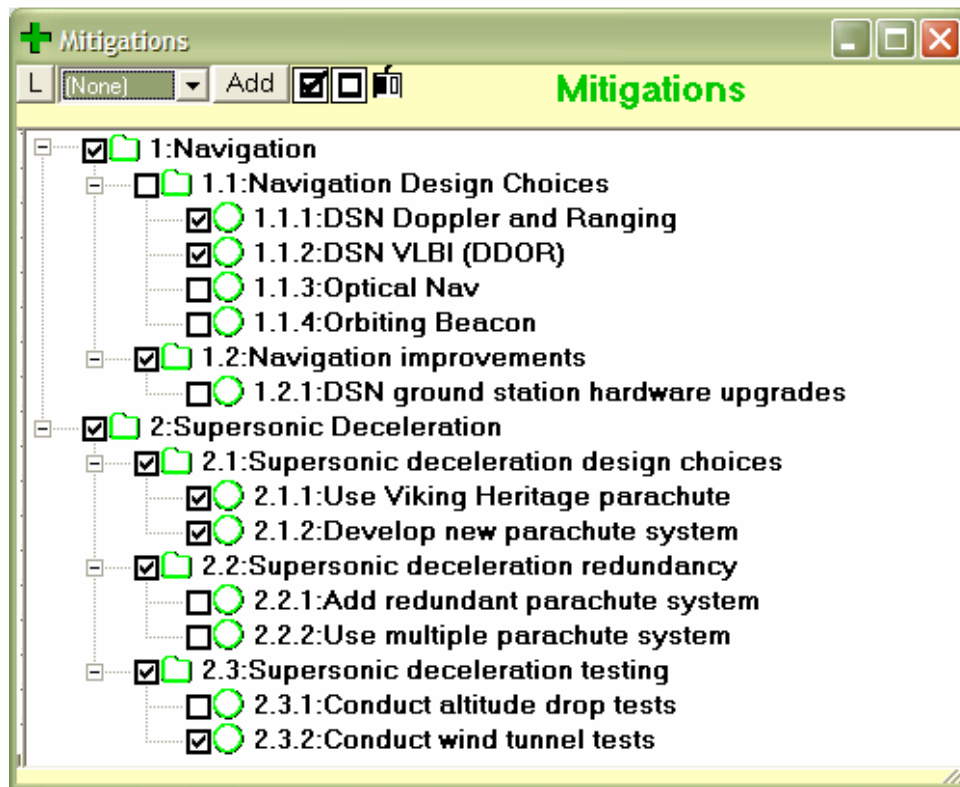
Figure 27: Mitigations of DDP Demonstration Model

The risk balance function of DDP is shown in Figure 28. As Design Switch Mitigations are selected, the risk bars show the relative risk associated with the selected design options. DDP has the ability to hold a particular setting as a baseline against which comparisons can be made by selecting alternate options.
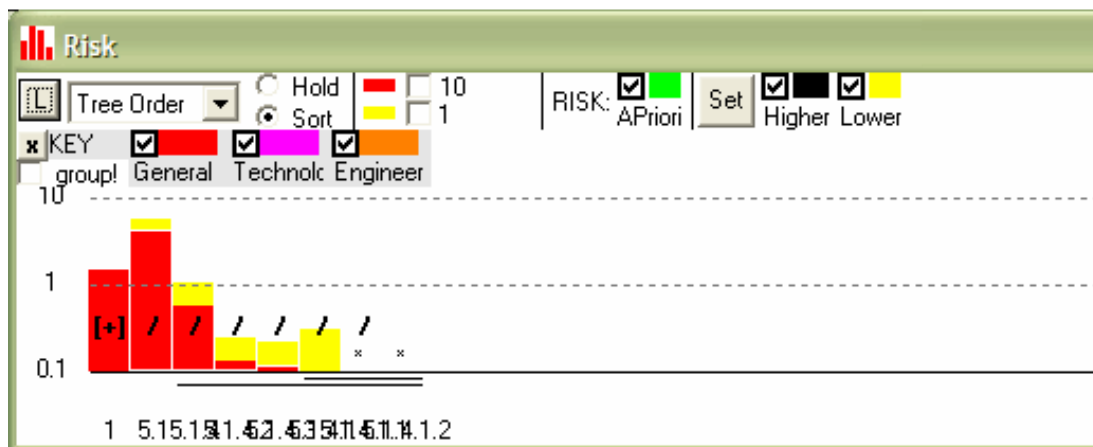
Figure 28: Risk Balance of DDP Demonstration Model

Objective attainment can be viewed in a manner similar to the risk balance. Figure 29 shows the objective attainment function for the demonstration model.
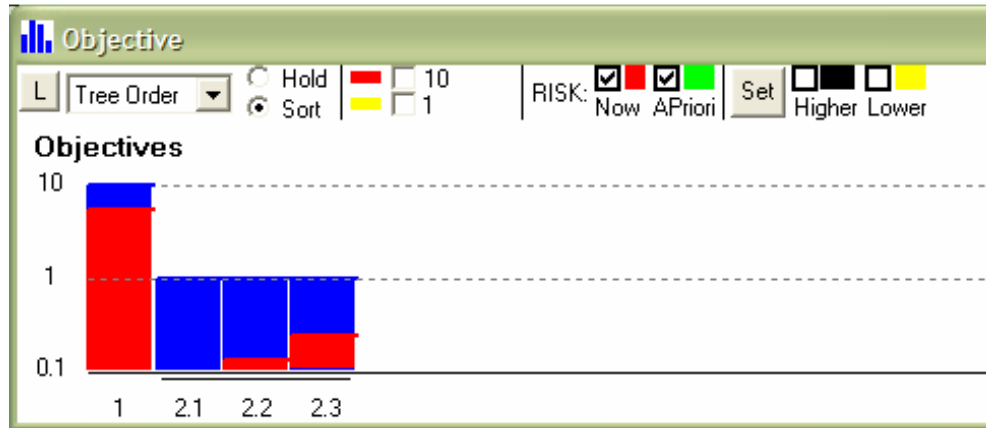
Figure 29: Objective Attainment of DDP Demonstration Model

5.4.2 Use of DDP in a Design Setting

The Team X conceptual design team at NASA JPL uses high level design tools operated by subsystem experts to converge on a spacecraft design for a given set of high level requirements. This type of design environment is characterized by:

◇ Rapid trades

◇ Solutions that are near-optimal and not exact

◇ Reliance on expert opinion

◇ Informal design flow

◇ Varying levels of detail

An EDL DDP model can add value to the design process in this type of setting. Once a DDP model is created and populated with data, trades can be made rapidly. In Team X, the risk chair and/or EDL chair could operate the DDP model during a design session. Knowledge of the relative amount of risk associated with the objectives for various design options provides useful information for making design decisions.

Trades can be made manually by selecting and deselecting mitigations. A morphological matrix of design alternatives, shown in Figure 30, can be used to aid users with design tradeoffs. In a conceptual design setting, the morphological matrix would contain the possible design choices captured in the DDP model. The matrix would serve as a roadmap of options that the user could choose amongst and trade off.

Subsystem	Category	Alternative 0	Alt 1	Alt 2	Alt 3	Alt 4
Approach Navigation			Doppler and Ranging	Optical	Delta-VLBI	Orbiting Beacon (2-way Doppler to orbiting s/c)
Entry Navigation			IMU	Doppler ground speed	Surface Beacon (2-way Doppler and range)	Terrain following
Orbital Navigation		None	DSN			
Aeroassist		None	Propulsive Orbital Insertion	Aerocapture	Aerobraking	
Cruise Stage		None	Cruise stage			
Spacecraft Attitude Control	Spin Stabilized		Passive spin	Spin with precession control	Dual spin	
	3 Axis		Passive 3 axis	Active 3 axis		
Communication	Cruise Bandwidth		S-Band	X-Band	Ka-Band	Ku-Band
	Cruise Antenna		LGA	MGA	HGA	
	EDL DTE Bandwidth		S-Band	X-Band	UHF to orbiting asset	
	EDL DTE Antenna		LGA	MGA	Patch	
Hypersonic Decelerator		None: Passive	Attached ballute	Trailing ballute		
TPS	Ablating		SLA-561	PICA	Carbon Phenolic	SIRCA
	Non-ablating		TUFROC	Carbon-carbon Genesis type	UHTCs	
Guided Aeromaneuvering		None	Tabs	Active control surfaces	Cg control	RCS
Drogue Parachute		None	Single drogue			
Supersonic Decelerator	Number	None	Single parachute	Triple parachute		
	Type	None	Viking Heritage DGB	New DGB	Parafoil	Steerable parachute
Altitude and Velocity		None	Radar Altimeter	Descent Imager		
Subsonic Decelerator		None	Use supersonic chute	Single parachute	Triple parachute	
Flight System		None	Airplane	Balloon		
Powered Descent and Control		None	Rocket assisted	Transverse motors		
Hazard Avoidance		None	LIDAR	Optical		
Touchdown System		None: Penetrator	Energy absorption	Propulsive with legs	Airbag	

Figure 30: Sample Morphological Matrix

A continuum of trades can also be considered automatically using the optimization feature of DDP. After defining the objectives as desired, a user in a design setting could use the optimizer to find the best design (in terms of a risk/cost tradeoff) among the available design options.

The taxonomies feature of DDP allows for sets of design options to be switched on and off within the model. For example, a taxonomy could be created that switches on all the necessary risk and mitigation elements for the model to reflect the MER missions. Designers could then use MER as a baseline to assess a future mission that is similar to MER but has some unique aspects.

A DDP model meets the flexibility and ease of expansion requirements for the proposed methodology. DDP allows for the user to easily make adjustments to existing, or add new, objectives, risks, and mitigations. New technologies, improvements to existing hardware, and reductions in uncertainty are easily accommodated by DDP.

5.4.3 Known Challenge with the Methodology

A problem exists with the use of Design Switch Mitigations and logical fault trees within DDP. Recall that Design Switch Mitigations work by activating a risk with zero a-priori likelihood with a negatively scored mitigation, thus inducing likelihood on the risk. The problem occurs only when two or more risks are under an AND gate and one of those risks is activated using a corresponding Design Switch Mitigation as depicted in Figure 31. When only one risk is activated, the overall likelihood at the gate level is diluted since the likelihood of the other risk (a-priori) is equal to zero. This prevents accurate calculation of risk and accurate optimization of mitigations.
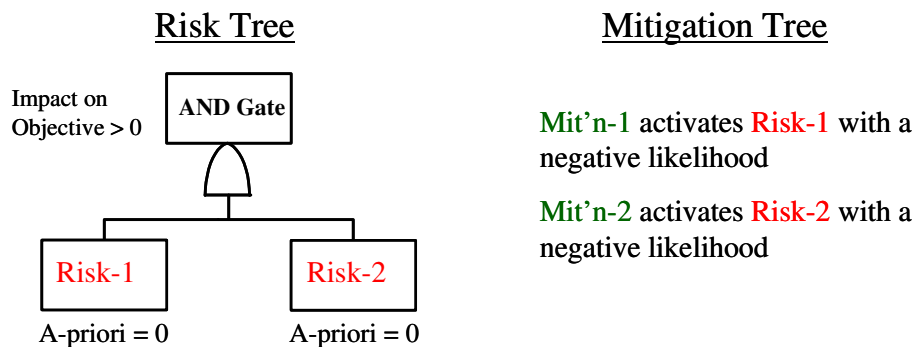

Figure 31: Known Challenge with Methodology

5.4.4 Possible Improvements to DDP as a Conceptual Design Tool

DDP is a powerful risk management tool, particularly for assessing risks and mitigations of a fixed system or technology. This section presents some possible improvements for

DDP in a conceptual design process, where the system is dynamic and risks are linked to design choices.

The use of Design Switch Mitigations and Improvement Mitigations is somewhat complicated. Furthermore, the previously discussed problem arises when Design Switch Mitigations are used in conjunction with logical fault tree AND gates. Explicit differentiation of Design Switch Mitigations from Improvement Mitigations could help alleviate these issues. This explicit differentiation is envisioned as a new element called Design Solutions that is added to the objectives, risks, and mitigations triad. The Design Solutions would essentially be Design Switch Mitigations. All mitigations would then be the traditional DDP mitigations (Improvement Mitigations), while the Design Solutions would be used to switch on and off risks. The underlying program code of Design Solutions could also be written such that the problem with Design Switch Mitigations and logical fault tree AND gates was solved. The algorithm could ignore unchecked risks under AND gates rather than consider them to have a zero likelihood.

The ability for DDP to accept data from nearly any source is a great asset. Scoring the risks against the objectives and mitigations against the risks might be improved by allowing the user to enter distributions rather than point values. Because the data can come from a variety of sources and quantifies a diverse variety of factors, some of the values may be known to a greater certainty than others. The distributions would allow for DDP to capture the degree of certainty in each data point, and would also allow for calculation of risk distributions showing confidence in the risk output. A drawback to this possible improvement is that it increases the time and effort required to mine and enter the data.

DDP can currently import the objective by risk and risk by mitigation matrix values from a comma delimited file. It may be useful in a conceptual design setting to import values from other software tools. For example, JPL Team X makes extensive use of Microsoft Excel worksheets linked through the ICEMAKER data transfer program during a design session. Linking the DDP inputs to these established tools could make for a powerful combination.

In arriving at a final conceptual design, many different design combinations are considered. To facilitate the comparison of many different designs at once, a trade organizer functionality could possibly be added to DDP, whereby objective attainment or risk balance windows for several different design configurations may be tiled next to each other for comparison.

5.5 Summary

A risk evaluation methodology was developed in response to a need for early assessment of EDL risk in the spacecraft design process. The methodology satisfies the specific goals of this task. The procedure and rules for implementing the methodology were outlined for easy repetition. A DDP demonstration model was created to show how an EDL risk model might be created and used for rapid design trades. Finally, some

possible improvements for the use of DDP in a conceptual design setting were presented.

5.5.1 Achievements

A generic EDL risk architecture was created and used as a foundation for a DDP risk model. The DDP risk model accomplishes the goal of facilitating tracking and visualization of EDL technical risks. Furthermore, the DDP model, together with the Morphological matrix of alternatives and ESDs, provides a road map for EDL mission design.

5.5.2 Recommendations for Future Work

While it was not within the scope of this task to quantify the DDP EDL risk model with real data, quantification of a portion of it would be beneficial for assessing the methodology. The solicitation of further EDL expert opinions would also be worthwhile. Finally, the DDP model could be tested in an actual conceptual design environment to demonstrate its added value.

6 Radiation Protection and Shielding Task

6.1 Introduction

As has been noted elsewhere [15], space radiation is a major problem for long duration space exploration with humans and robots. There are no known countermeasures for repairing or avoiding radiation damage except to reduce the strength of the radiation field inside the spacecraft. Again, there is only a single solution that has yet been implemented, which is to add mass. This problem of mass addition dramatically raises the stakes in radiation-resistant spacecraft design.

Mass addition in a spacecraft has been heretofore an ad hoc solution to the radiation problem. However, an optimal solution would be to make the most of existing and required mass on a vehicle (i.e. propellant tanks, environmental control and life support system water supplies, bulkheads, etc.) to protect the crew before adding mere ballast. The first phases in spacecraft design have the widest ranges of design variables available, and hence the most design freedom and control, so it makes sense to apply effort to supporting radiation analysis at this level of development.

Part of the problem of doing radiation analysis at the earliest design levels is that the design is in a great amount of flux. Any model of the design is still more or less a sketch, subject to great changes. The design studies at this point are not simply tweaks of a few parameters that describe the design. Rather, they are arguments as to the basic structure of the vehicle, with discussions like: winged orbiter or capsule? nuclear or solar power? crew and cargo separated or together? These types of design arguments are not amenable to thorough modeling and analysis – many parameters are still unknown.

In the face of so much uncertainty, how is it possible to make a reasonable estimate of the properties of the future design that rely so much on geometry? Part of the answer is that at this stage, an optimum value is not sought. What is sought is the direction in which the design must go in order to converge to the optimum value as the design process proceeds to its end. After all, if the results can be exactly determined from the outset, what is the point of detailed design and test? It must be emphasized that the previous statement does not lead the reader in the direction of giving up, but to change expectations as to the goal of evaluating "detailed properties" of an early-stage design.

The Aersospace Systems Design Laboratory has long wrangled with the issues of needing to run analyses that require geometry at a time that detailed geometry cannot be made available. An example solution is the use of Ames Research Center's Rapid Aircraft Modeler [16] that is used in ASDL in order to define preliminary geometry for aerodynamic analysis. Rather than a CAD model of lofts and curves, the Rapid Aircraft Modeler takes as inputs design variables such as wing sweep and engine inlet location and size. The geometry is not exact or optimized, but is a sufficient approximation for basic panel and drag estimation methods. This allows a configuration designer to very

rapidly create sketch forms of the aircraft of interest, without knowledge of CAD tools. In addition, it allows for all of the alternatives to be evaluated on their own merits.

A similar approach has been investigated for radiation design, enabling a rapid survey of different configurations and their quality with respect to protection for humans and robotics.

6.2 Approach

The approach can be best understood by looking at a general procedure for analyzing radiation on an existing design, exemplified by work on the International Space Station [17]. The importance of geometry to radiation analysis is paramount, as it determines the distribution of mass (and what type of atoms) each ray must penetrate in order to reach a vulnerable cell or circuit.

The analysis usually begins with a CAD model of some kind. A point of interest inside the vehicle is chosen, and imaginary rays are cast from this point in all directions, meant to "feel out" the paths of incident radiation. Ray-tracing routines require a model to have some mesh representation, so this is another step is the procedure. Once the rays have found the composition and mass of the material between the point and free space, then transport calculations can begin. Transport calculations transform the free space radiation spectrum into a radiation spectrum at the point of interest. These calculations typically account for all reduction in incident radiation, as well as new radiation generated by fragmenting the atoms that make up the radiation shielding. Finally, the nature of the target (humans or robotics) of interest is used to determine how much harm the internal spectrum causes.

The general approach taken in this paper is a reductionist one. Other approaches are often synthetic in nature, attempting to construct an integrated package to solve all components of a given problem. For example, multiphysics solvers like Ansys strive to enable users to generate geometry, mesh and solve multiple problems (thermal, structure, fluid) upon the same geometry. These solutions are good for precise, interconnected solutions of aerothermal (planetary reentry) and aeroelastic (wing rigidity) problems. At the initial stages of design, these solvers suffer from "too much information."

```
                    ┌──────────────────────────┐
                    │      CAD Model Built      │
                    └──────────────────────────┘
                                 │
                                 ▼
              ┌────────────────────────────────────┐
              │     FEM Geometry Representation     │
              └────────────────────────────────────┘
                                 │
                                 ▼
                  ┌──────────────────────────┐
                  │   Material specification  │
                  └──────────────────────────┘
                                 │
                                 ▼
                  ┌──────────────────────────┐
                  │  Wavefront format transfer │
                  └──────────────────────────┘
                                 │
                                 ▼
                  ┌──────────────────────────┐
                  │  XRadICal ray-trace of model │
                  └──────────────────────────┘
                                 │
                                 ▼
          ┌──────────────────────────────────────────┐
          │  Radiation transport analysis of ray-trace results │
          └──────────────────────────────────────────┘
                                 │
                                 ▼
                  ┌──────────────────────────┐
                  │   Human dose calculations  │
                  └──────────────────────────┘
```
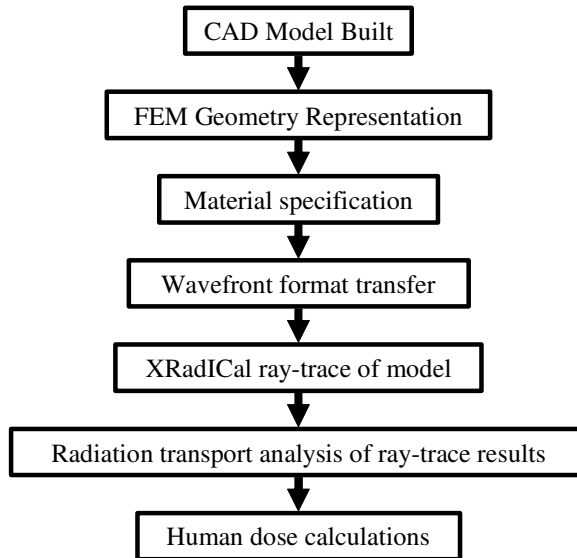
Figure 32: Existing radiation analysis pipeline for geometric models

The reductionist approach has two advantages. One is the simplicity of each individual tool, and the likelihood that it can be made to run rapidly and flexibly. The other is that it is possible to "shop around" to take existing analysis methods off the shelf and string them together. Note that the stringing together is not necessarily a trivial problem in most cases, hence the attempts to make an all-in-one package. Yet, for the situation of early stage design, a very useful and suitable solution is the use of response surface functions or neural networks. These "metamodels" are an enabling technique for many types of collaborations, and have a well-established methodology surrounding their derivation and use.

One remark is that metamodeling at the early phases of design allow for the use of old methods in a brand new way. Traditional sizing equations for aircraft or engine design cycles are simple and of closed form. However, to reach closed form, many assumptions and simplifications are made, often hidden behind efficiencies or coefficients. It can be recognized that these equations give exact answers, *provided the efficiency factors are correct*. These efficiency factors are determined by detailed design parameters and the flight condition. With metamodels, however, these parameters can be wrapped to give the efficiency factors on the fly. Similar thinking led to the development of Stingray, which will be described later.

The approach outlined here recognizes that suitable and verified codes already exist for a bulk of the problem. For example, a rapid radiation transport code has been developed and validated at Langley over several years, named HZETRN (High charge (Z) and Energy ion TRaNsport). It also contains basic response functions for human tissue to a given cosmic radiation spectrum. Similar response functions have been

rendered into computer code for electronics recently. The only piece that is missing here is a rapid, simple to use geometry and mesh generator.

The problem of geometry and mesh generation is again non-trivial, especially the mesh generation portion. Attempts to 're-invent the wheel' would merely create yet another CAD package. It was decided to create a tool specifically suited to ray-tracing, in particular having a tool that could solve the ray-tracing equations in closed form. Avoiding the mesh step would save a great deal of time and remove the expertise requirement in operating the geometry tool.

It must be noted that the closed-form solutions of ray-tracing are only useful for early-phase design. They implicitly require the use of primitive shapes (prisms, spheres, cylinders, etc.), but this is not a great compromise in early design for spacecraft. Spacecraft tend to have simple shapes, and the internal layout in the early phases is usually defined only be a set of notional "keep out" areas of some estimated density.

To summarize, the approach used here was formulated by focusing on the characteristics of both traditional early phase design and tradition radiation analysis. By breaking the traditional radiation analysis down, it was seen that useful codes already existed for all functions but the geometry definition. These codes could be wrapped in metamodels without much loss in fidelity, and the metamodels used to obtain rapid and flexible results. A tool to create and ray-trace simple geometries is required to finish out the analysis of radiation for early-phase design.

All of the codes mentioned above will be outlined in the following sections, with an emphasis on the original work undertaken to build the geometry tool.

6.3 Implementation

This section outlines the adaptation of off-the-shelf codes and the development of new ones to build a radiation analysis pipeline for early phase design. Little modification was required to the original codes to enable the use of the response surface methodology.

6.3.1 High Charge (Z) and Energy ion TRaNsport (HZETRN)

HZETRN is the workhorse of Langley's radiation analysis procedures. It has been validated with respect to the Space Shuttle program [18], in addition to entailing a body of empirical transport knowledge. It has approximate, 1-dimensional variants as well as been the core of the RadICal CAD analysis procedure.

In general terms, HZETRN seeks to solve the flux problem of various ion species through an imaginary volume. The volume described in HZETRN is that of a sphere. If the flux problem is viewed as the form:

$$\phi income - \phi outgoing = \frac{\partial}{\partial t} \phi net$$

where ϕ represents the flux into a volume, then it can be written in the following form [19]:

$$\phi_j\left(\vec{x}+\partial\vec{\Omega},\vec{\Omega},E\right)\delta^2 d\Omega - \phi_j\left(\vec{x}-\delta\vec{\Omega},\vec{\Omega},E\right)\delta^2 d\vec{\Omega} =$$

$$\delta^2 d\vec{\Omega}\int_{-\delta}^{\delta}dl\sum_k\int\sigma_{jk}\left(\vec{\Omega},\vec{\Omega}',E,E'\right)\phi_k\left(x+l\vec{\Omega},\vec{\Omega}',E'\right)d\vec{\Omega}'\,dE'$$

$$-\delta^2 d\vec{\Omega}\int_{-\delta}^{\delta}dl\,\sigma_j\left(E\right)\phi_j\left(\vec{x}+l\vec{\Omega},\vec{\Omega},E\right)$$

where Ω is a surface normal of the differential surface element $\delta^2 d\Omega$,

x is the vector from the surface element to the sphere's center,

l represents length of travel between entry and exit surfaces,

E is ion energy,

and σ represents an interaction cross-section.

The cross section σ_{jk} represents all processes that transform a type k particle into a type j particle. The second term in the equation represents the source of secondary particles (e.g. fragments of collisions) that occur in the flux tube between the two surfaces. The third term represents the losses due to nuclear reaction (e.g. heavy ions lost in fragmentation).

Details on the expansion and simplification of these terms are given in a description of the HZETRN code [19]. In general however, the simplification is into a transport equation that calculates the loss of ion energy as it interacts with its target.

$$\left[\frac{\partial}{\partial x}-\frac{\partial}{\partial E}S_j\left(E\right)+\sigma_j\right]\phi_j\left(x,E\right)=\sum_{k>j}m_{jk}\sigma_k\phi_k\left(x,E\right)$$

$$\left[\frac{\partial}{\partial x}-\frac{\partial}{\partial E}S_j\left(E\right)+\sigma_j\left(E\right)\right]\phi_j\left(x,E\right)=\sum_k\int_E^\infty\sigma_{jk}\left(E,E'\right)\phi_k\left(x,E'\right)dE'$$

where S represents the stopping power, the change of energy per unit distance through a medium,

x is a length traveled along a ray,

E is energy,

σ is interaction cross-section

and ϕ is flux.

The top equation represents the transport equations of heavy ions, while the bottom one represents light ion transport. The top equation has a nuclear absorption term for heavy ions, while the bottom equation has a nuclear production term.

Relevant assumptions to highlight are:

◇ One-dimensional propagation – i.e., no spread of fragments or particle ricochets

◇ Continuous slowing-down – i.e., Coulomb forces are dominant interactions for ions

◇ Velocity is conserved after particle collision

With these approximations, and a nuclear cross-section database, it is possible for HZETRN to make useful predictions without resorting to a Monte Carlo scheme. Thus, it is already a fast-acting code, and is suitable for batch running to derive metamodels. As will be seen later, it is not quite fast enough for online execution on a ray-tracing model for every single ray, but is quite useful if runs are used wisely.

6.3.1.1 Changes for metamodeling

As stated before, HZETRN is more than fast enough to enable batch modeling. In addition, its approximations and examples of use at Langley show that it is feasible to decouple the analysis and the ray-tracing. No functional changes were required to fit into the metamodeling methodology.

The main change to the code was to enable batch execution by moving the inputs from the source code into external data files. Originally, the inputs would have to be changed in the source code and then recompiled before execution. Moving the required inputs and outputs to external files enabled for many cases to be run automatically. With DOS scripts to write and manage generated files, it became straightforward to run DoE cases to form the basis of the metamodels.

6.3.1.2 Single-event upset TRaNslator (SEUTRN)

SEUTRN was created to link HZETRN's transport calculations to a relatively simple electronics model. The electronics model, known as the sensitive volume method [20], is often used in early electronics estimates.

The basic argument of the sensitive volume method is that a particle leaves behind energy as it passes through a material. This energy is a function of the length of ray within the sensitive volume and a scaling coefficient known as the linear energy transfer. If more energy is deposited within the volume than the circuit's threshold for switching, a bit reverses state or is upset. The parameters of critical charge (which can be transformed into threshold linear energy transfer) and volume dimensions are used to transform radiation fluxes into expected bit error rates.

In addition to heavy ion calculations, SEUTRN also uses an approximation for proton-induced upsets that is illustrated in [21]. The approximation is mostly empirical, as proton-induced upsets have different physics involved (direct collision) from ion-induced upsets.

Like HZETRN, SEUTRN required only changes in the way input and output are handled.

6.3.2 Stingray

As discussed earlier, metamodeling can be combined with traditional, first-principles type equations to provide rapid and accurate design results. This is the thinking behind Stingray, which calculates the closed form solutions to the so-called ray-tracing equations. Essentially, a ray is a parameterized line in three-dimensional Cartesian space, with the simple equation

$$\vec{p} = \vec{u} + \vec{v}t$$

where p is the point of interest,

u is the ray starting point

and v is the unit vector of the ray's projection.

Typically, a ray-tracing engine uses branching and subdivision algorithms to locate the point of intersection between a ray and a surface, as well as the angle of intersection. Many surface parameterizations have been derived and described in the field of computer generated graphics over the years. The very first of these surfaces were the basic, primitive shapes (cubes, spheres and cylinders) that could be easily solved by simple computers.

The solution of the ray-tracing equations for these basic shapes is an intuitive method. First, the surface parameterization such as

$$x^2 + y^2 + z^2 = r^2$$

for a sphere has its x, y and z values substituted by the parameterization of the ray:

$$\left(u_x + t\cos\theta\sin\phi\right)^2 + \left(u_y + t\sin\theta\sin\phi\right)^2 + \left(u_z + t\cos\phi\right)^2 = r^2$$

The terms are then expanded and solved for t, the distance along the ray that the intersection occurs.

In the approach section, the current pipeline for radiation analysis at Langley was described. As in graphics ray-tracing, the goal is to 'feel out' radiation sources from a point of interest, rather than shooting all possible rays into the scene. For the XRadICal software, each point of interest has a distribution of rays that are even over a virtual sphere. Stingray uses a similar distribution.

To get an even distribution of rays simply, the rays were parameterized in spherical coordinates, which renders the ray-trace equation into the form shown above.

For a sphere, the solutions of t are

$$t = -\left(u_x\cos\theta\sin\phi + u_y\sin\theta\sin\phi + u_z\cos\phi\right)$$
$$\pm\sqrt{r^2 - \left(u_x^2 + u_y^2 + u_z^2\right) + \left(u_z\cos\phi + \left(u_x\cos\theta + u_y\sin\theta\right)\sin\phi\right)^2}$$

The solution of t for a plane is

$$t = -\frac{a(u_x - x_0) + b(u_y - y_0) + c(u_z - z_0)}{a \cdot \cos\theta \sin\phi + b \cdot \sin\theta \sin\phi + c \cdot \cos\phi}$$

Finally, the solutions of t for a z-axis aligned cylinder are

$$t = -\left(\frac{u_x \cos\theta}{\sin\phi} + \frac{u_y \sin\theta}{\sin\phi}\right) \pm \frac{\sqrt{\left(2r^2 - u_x^2 - u_y^2 + \left(u_x^2 - u_y^2\right)\cos(2\theta) + 2u_x u_y \sin(2\theta)\right)\sin^2\phi}}{\sin^2\phi\sqrt{2}}$$

The result for a cylinder is simple, but it is only good for a cylinder that is oriented along the z-axis. Also, the cylinder has infinite height and no ends. This brings up the need for some manipulations of the equations and solutions in order to gain results that are physically useful. One solution to this problem is to rotate and move the rays so that they have the same relative orientation to the cylinder that they would if the cylinder was in the desired orientation. Since the program is only solving for distance along the ray that intersection occurs, this will automatically find the points of intersection in the original problem.

Another required trick is to screen the results so that the cylinder has both a finite height and closed ends. Removing solutions behind the height of the cylinder is straightforward, and the end intersections are found through an intersection with a circular plane.

With closed-form solutions in hand, Stingray can then use the intersection data to calculate the effective shielding surrounding a point. Objects are specified with a given material (either water or aluminum for the simple example, but others can be implemented easily when properties are known) and whether or not the object is solid. If it is solid, Stingray looks to solve the distance traveled through the shape. Otherwise, intersections are simply counted and multiplied by a shell thickness.

For simplicity, the intersections on each shape are placed onto a separate array. When the intersections are known, these arrays are operated on to find effective shielding thickness. Once the shielding thickness is calculated, the arrays corresponding to individual shapes are merged to form a total shielding thickness as seen from the current point of interest.

When the total shielding is known, this is when the metamodels come into play. From the point of view of Stingray, it does not matter what model or data is used to generate the response surface. Stingray answers the question of how much shielding stands between the open environment and the material (cells or circuitry) of interest. The response surface equations are used to relate this value to an effect of interest.

Stingray can have a library of response surface equations for various external environments, shielding materials and metrics of interest. Once the shielding thickness tables are generated, any metamodelled response could be cycled through quickly. An example would be the stepping through various phases of the solar cycle, determining best, worst or root mean square galactic radiation exposure throughout a mission.

6.4 Demonstration

6.4.1 Metamodel Reduction

The bridge between Stingray's ray-tracing routines and useful radiation analysis is the use of metamodels. These metamodels can either bridge analyses or be used as a way to distill expert knowledge for the purpose of communication (the expert is still needed to authenticate and guide the metamodel usage). Those familiar with the metamodeling technique may skip this section and move to the discussion of Stingray's use on demonstration cases. This section is meant to provide a concrete example on the derivation and fit-checking of response surface functions. Note that these functions can be tied to other analysis methods or used in a standalone fashion – as part of an Excel spreadsheet, for example.

For demonstration purposes, the response function of single-event upsets (SEU) is derived for a general spacecraft. Previous work on the SEU problem ([20],[21]) shows that there are six variables of interest at the top level:

◊ Shielding thickness (in this case pure aluminum of varying densities)

◊ Silicon thickness (included as a target for post-shielding radiation)

◊ Critical charge for an electronic component

◊ Sensitive volume cross-section (assumed square)

◊ Sensitive volume thickness

◊ Proton sensitivity apparent threshold

The first step in reducing a metamodel is to specify a Design of Experiments, which will maximize knowledge of the response with a minimum of "experiments" (in this case, numerical). The statistical package JMP is the usual tool of choice for specifying how many runs to use at which settings. A fifty-four case Box-Behnken design was used in this example. This DoE spans the design space identified in Table 4.

Table 4: Design of Experiment ranges

	Al Shield (g/cm²)	Critical Charge (pC)	Cross Section (μm2/bit)	Thickness (μm)	Sensitivity Threshold (MeV)
Min Value	0.1	0.05	0.4	1	5
Max Value	10	0.15	1	4	80

With the run settings specified, a set of MATLAB scripts and DOS batch files was used to execute HZETRN, LETTRN and SEUTRN and develop a database of responses

and inputs. Once the database was built, it was brought into JMP in order to develop the response surface equations.
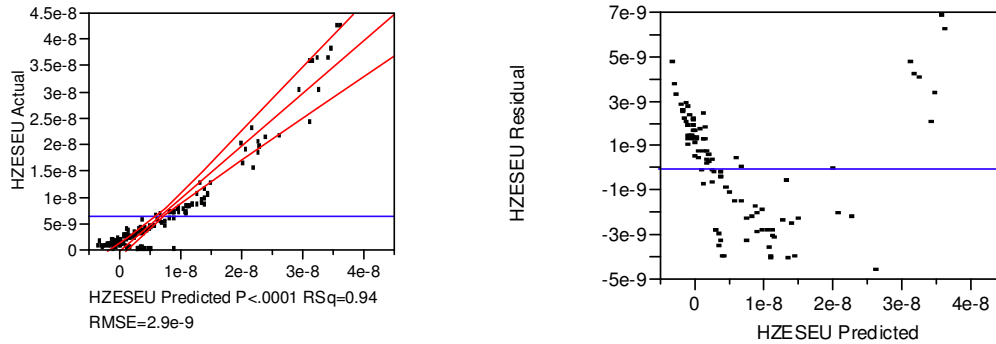

Figure 33: Actual by Predicted and Residual by Predicted plots of HZE SEU response

Since the response surface equation is a linear equation and terms of the b coefficients:

$$R = b_0 + \sum_{i=1}^{k} b_i x_i + \sum_{i=1}^{k} b_{ii} x_i^2 + \sum_{i=1}^{k-1} \sum_{j=i+1}^{k} b_{ij} x_i x_j \qquad i \neq j$$

it is relatively straightforward to do a least-squares fit upon the database to derive the coefficients.

Once the co-efficients are obtained, a series of statistic tests is applied to evaluate the fit. The first a simple look at the R^2 value to see how well the equation correlates to the data. The next is to look at the actual-by-predicted and residual-by-predicted plots to see if there are any regions or patterns of poor fit. If there are patterns, there some options to reformulate the response surface to try and correct. These actions include adding higher-order (in terms of x) terms or applying a mathematical transformation to the response. For this example, it was found that applying the response equation to the natural logarithm of R, rather than R itself, led to better fitting. This can be seen by comparing the plots in both Figure 33 and Figure 34. It can also be seen that the transformed response has a more evenly distributed error by looking at the two residual by predicted plots.
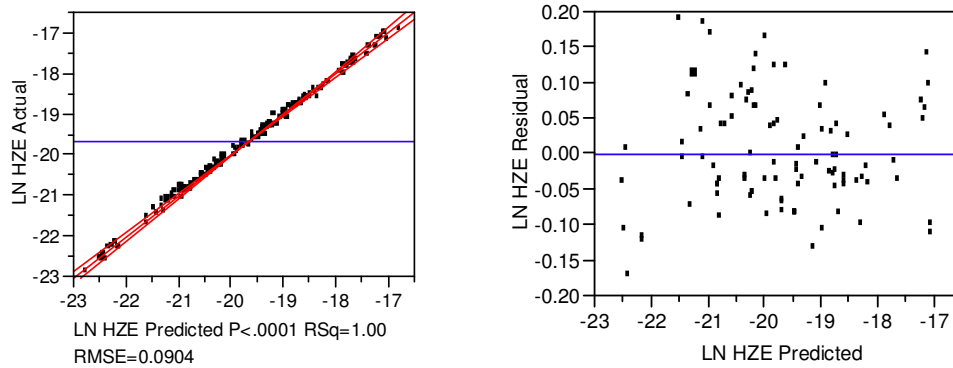
Figure 34: Predicted fit plots of natural log HZE SEU response

The next two tests are the model fit and model representation error. The model fit error quantifies the maximum and nominal errors between the response surface and its underlying database. The model representation error involves running extra validation cases taken at random points in the design space. The model representation error aims to quantify the maximum and nominal errors between the response surface and any true response it is meant to represent. The key aspects of Figure 35 to examine are the mean, standard deviation and span of the distributions. A well-fit equation will have symmetric, small errors and an approximately normal distribution. As seen below, the expected error at any point of the response surface evaluation is contained absolutely to plus or minus twenty-two percent. While not adequate for detailed design work, it is usable for early-phase design, especially considering that the response spans two orders of magnitude of upset rates.

Altogether, 164 iterations of running HZETRN, LETTRN and SEUTRN were performed to fit and check the response surface equations. Running in an automated fashion on a Pentium 4 PC, these cases took roughly one hour of execution.

It is worth noting that while the metamodels are used in this report as a core element in a Stingray evaluation, they can also be used in a stand-alone fashion. For example, a basic Excel spreadsheet that is meant to span various electronics part parameters can be fashioned for use in a design process.

Quantiles (left)

100.0%	maximum	18.70
99.5%		18.70
97.5%		13.40
90.0%		9.16
75.0%	quartile	5.60
50.0%	median	1.67
25.0%	quartile	-5.15
10.0%		-10.45
2.5%		-16.34
0.5%		-17.43
0.0%	minimum	-17.43

Quantiles (right)

100.0%	maximum	21.95
99.5%		21.95
97.5%		16.71
90.0%		9.67
75.0%	quartile	5.45
50.0%	median	0.61
25.0%	quartile	-6.36
10.0%		-11.15
2.5%		-17.42
0.5%		-19.89
0.0%	minimum	-19.89

Moments (left)

Mean	0.2923458
Std Dev	7.6237629
Std Err Mean	0.7585928
upper 95% Mean	1.7973722
lower 95% Mean	-1.212681
N	101

Moments (right)

Mean	-0.130191
Std Dev	8.3479247
Std Err Mean	0.6518634
upper 95% Mean	1.1569949
lower 95% Mean	-1.417376
N	164

Figure 35: Model Fit and Representation error statistics.

6.4.2 Stingray Ray-Trace and Metamodel Evaluation

There are two examples here to demonstrate the use of the Stingray code. The first is a sample space probe with interest in data recording and processing circuits. The second is a sketch of a Crew Exploration Vehicle with large supplies of propellant and water onboard. The only materials available in the versions of HZETRN released to Georgia Tech were water and aluminum, so the analogues may be stretched. Thus, it is important to look mostly at the technique, as opposed to the applicability of data available to the demonstration use.

The layout of the space probe is given below in Figure 36. It is a simple and cubic, with solar panels and two decks upon which to place internal components. All of the hardware is modeled as aluminum, with differing densities on components so that they do not appear to be solid blocks of metal.
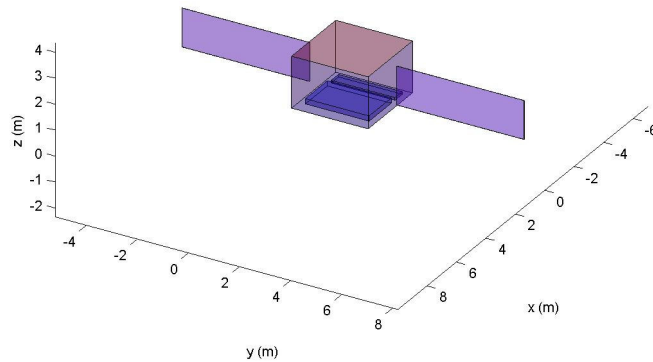
Figure 36: Space probe layout

All of the materials in the space probe are modeled as aluminum, which is a stretch for most of the components. By adjusting the bulk density of the components, however, it is reasoned that the approximation is good enough for a demonstration of the overall method. The majority of aluminum is found in solar panel backing and the electronics and power module housings. This caveat is meant to help the reader recognize that the ray-trace methodology does not change for this limitation in materials modeling. From the Stingray point of view, it is a matter of producing response surfaces that are capable of modeling the materials appropriately. This also helps to illustrate a potential "hot swap" capability, where response surfaces for different materials are brought in as a wider library is developed.

In order to produce the results of Stingray, a four-pi sterradian (full sphere) pattern of rays was spread in each direction, with 169 rays used to represent the sphere. Many of these patterns were placed on a grid inside the probe housing to sample the radiation field inside the entire probe. Once the shielding experienced by each ray was calculated, a response surface equation representing the electronics was used to transform shielding into electronic effects. The resultant SEU rate along each ray of the distribution was averaged together with each other, forming a scalar SEU rate at that one point. Again, this was iterated over many points inside the probe to develop a field.

For this case, a part was specified with a threshold linear-energy transfer of roughly $10 \text{ MeV*cm}^2/\text{mg}$ and a saturation cross-section of 10^{-7} cm^2.

The results were taken together and plotted in Matlab, and can be seen in Figure 37. A false-color plot is used to highlight areas of relatively high and low SEU rates. Since

the largest concentration of mass is currently on the bottom shelf (the two boxes in the configuration are battery and distribution boards), it is expected that the lowest radiation would be seen near the deck. As expected for a typical spacecraft, the placement of the electronics boards alone is not a panacea for radiation effects mitigation. However, these results are showing a roughly fifteen percent mitigation effect through intelligent placement of components. This effect cannot be entirely neglected, especially if there are several high-density components that could be strategically re-configured to obtain an inexpensive reduction in error rates on a sensitive part.
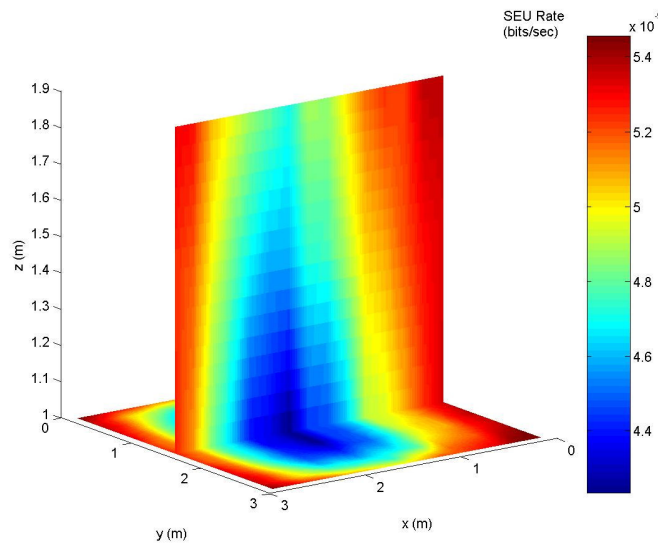

Figure 37: Space probe expected single-event upset field

The second example is a crewed space vehicle. This is also an example of using Stingray to estimate the influence of the "heavy hitters" in a design. Since this is meant as a demonstration for early-phase design, it is a legitimate strategy to only include the elements that should have the greatest effect. For a human mission, the main elements of the spacecraft that can be moved around are water storage tanks and propulsion tanks.

For test purposes, two layouts are shown. The first, shown in Figure 38, has a water tank forming a ring around the exterior of the spacecraft. The second has a water tank stacking vertically with the cabin. Otherwise, they are identical. In both cases, water was rationed for twenty days for a crew of six and six liters per day for each crew member. It is worth noting that water is very useful as a multi-purpose shielding material, since large amounts of it will be required by a spacefaring crew. For this case, the addition of water did not make any single ray penetrate more than 70 g/cm^2 of equivalent aluminum shielding. This is considered by the author to be a reasonable limit on the amount of

water shielding, since the upper bound on a ray for a Shuttle shielding study was 100 g/cm^2 of equivalent aluminum [22].
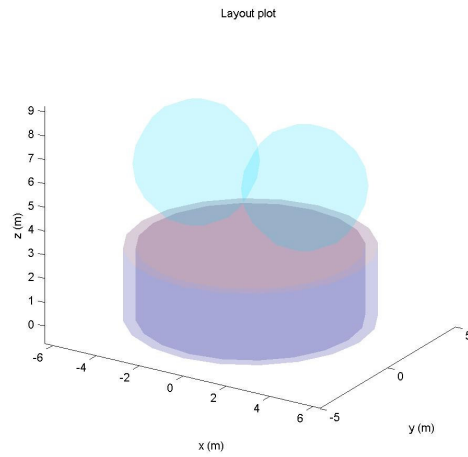

Figure 38: Stylized CEV layout

The dose field for the A configuration is shown in Figure 39. The largest source of shielding mass in this case appear to be the liquid hydrogen tanks, which are filled in this particular model. There is a slight abuse of the water material conversion in this case, but the density of the tanks was set to match that of liquid hydrogen, rather than
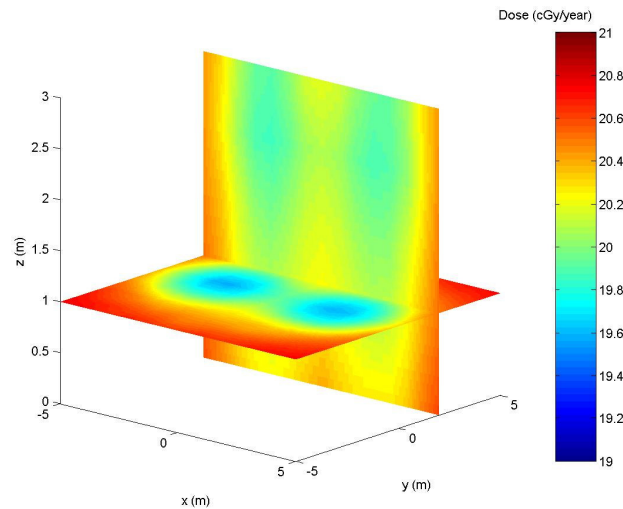

Figure 39: CEV configuration A dose field

water. If anything, this is a conservative estimate, as HZETRN studies of LH2 versus water for shielding show that LH2 is a superior shield on a mass-per-mass basis [19]. A potential suggestion from this result, even though water placement was the initial direction of the example study, is that it may be advantageous to have propellant
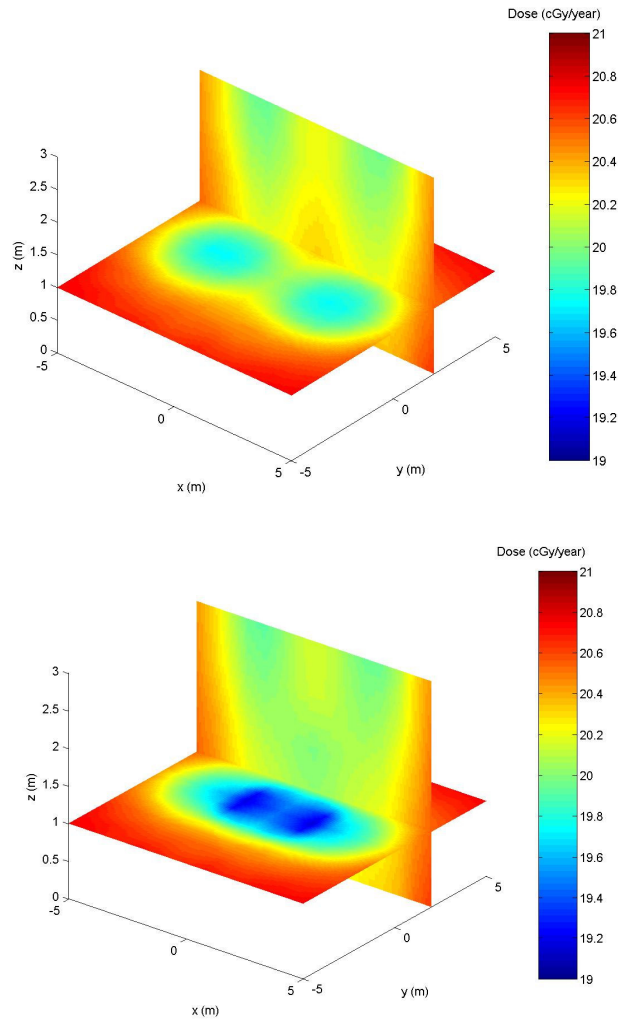

Figure 40: CEV configurations B and C dose field

shadow a larger solid angle of the cabin, via splitting of the tanks.

The dose field for the second CEV configuration is roughly the same as that of the first. It may be seen that there is a small improvement due to the reconfiguration, but again the hydrogen tank effects are dominant. If the hydrogen tanks are considered unmovable, one potential action is to try and build a 'storm shelter' configuration, shrinking the water tank radius to increase its thickness to maintain the same volume

(and thus mass). It can be seen from Figure 40 that there is indeed some benefit, but other trades would have to be made to determine the merit of this change.

This concludes the demonstration of Stingray for evaluating a radiation field inside a geometric body.

6.5 Summary

The work performed for Engineering of Complex Systems was meant to show how a preliminary design process could be enriched through the use of metamodeling and computational speed. The driving goal was to increase the amount of downstream knowledge available to an early designer, in order to make more informed decisions on major design parameters. Stingray is an example of a tool that changes the traditional focus of a detailed analysis to an informer of preliminary trade activities.

Since preliminary trade is hazy and rapid, those aspects were leveraged to design a rapid methodology based on closed-form solutions to the ray-tracing equation. These solutions were then coupled to an effects library of response equations to evaluate the desirability of various design choices from a radiation standpoint.

6.5.1 Achievements

Two major outcomes were achieved for this paper. The first was the adaptation of a series of legacy codes to the task of generating response surface equations. This was fairly simple, but it is also worth noting that a number of details about code execution and radiation analysis had to be learned in order to translate analysis parameters into electronics design parameters. The main example is the translation of sensitive volume parameters such as critical charge and volume dimensions into part data sheet parameters like threshold linear energy transfer.

The second task was the development of Stingray. While it remains unvalidated, the ray-tracing algorithm has been verified through multiple inspections.

6.5.2 Lessons Learned

A major lesson that is worth pointing out is that many of the current radiation analysis methods are already well-suited for metamodeling. There are no internal constraints in the transport program, nor are there any points at which the code "zeros out" or provides any other discontinuities. These discontinues disrupt response surfaces and require seeding of cases along the discontinuity in order to use metamodels such as neural networks.

With a relatively well-behaved toolset, radiation analysis does not face many of the challenges that such disciplines as structural analysis have faced in order to be brought into the interactive, collaborative method of design. This is good, as little investment in

the radiation tools that are deemed acceptable is required to bring their knowledge into earlier parts of the design process.

Another lesson to point out is the perennial requirement in collaboration for the partners to speak the same language. Biologists will have needs to specify results in various measures such as dose and biological equivalent dose (a quantity whose definition is still evolving to the author's knowledge). Electronics engineers, on the other hand, are more comfortable talking about linear energy transfer threshold, saturation cross-section and lifetime dose (as these quantities are in existing part specification sheets). This is simply something to keep in mind when negotiating inputs and outputs.

6.5.3 Recommendations for Future Work

The recommendations for future work take on two different directions. The first is in the area of collaboration. Variables of interest and basic, limited tools have been identified for conceptual radiation analysis. The next step is to work out the logistics of requesting, building and transferring metamodels from one NASA center to another. The use of metamodels for this collaboration has the benefits illustrated in this section of rapid execution and flexibility. In addition, it must be noted that this flexibility is completely in the hands of the expert that derives the metamodels. The expert can give as much or little flexibility as desired, so as not to give the inexperienced user "enough rope to hang himself."

The metamodeling example provided earlier serves as the basis for a trial – having the experts execute and analyze results of a batch of Design of Experiment runs, then reducing a metamodel that is believed to be appropriate. This metamodel could then be used by a designer (although not a radiation expert, but perhaps an electronic systems designer) at another center to play "what if" games by changing either the average shielding level or electronics parameters. An Excel spreadsheet will be provided that shows just such a metamodel, with the caveat that it was not generated by an expert.

The second area of suggested work is to continue with existing efforts in building flexible CAD-based analyses for radiation. As CAD packages become more intuitive, a sketched-out design could be used directly in the place of Stingray. In addition, collaborative design centers such as JPL's Team X currently provide clients with a CAD model for illustrative purposes. Such a model could be used to increase design knowledge as the appropriate tools to do so come online.

7 Conclusions

ASDL researchers developed and demonstrated approaches to incorporating discipline-level knowledge into the early stages of the space systems design process. The development took place in close collaboration with NASA experts at Langley Research Center and at the Jet Propulsion Laboratory.

Four areas where the space systems design process can be enhanced were explored: by integrating risk models into the early stages of the design process, and by including rapid-turnaround variable-fidelity tools for the key disciplines of reentry aero- and thermodynamics and radiation protection and shielding.

Efforts in each area resulted in a demonstration application and recommendations for future research.

8 References

[1]   A Vision for Space Exploration. The White House, Washington, D.C., January 2004. Web-published: http://www.whitehouse.gov/space

[2]   The Project Design Center. Jet Propulsion Laboratory, August 2004. Web-published: http://pdcteams.jpl.nasa.gov

[3]   JMP website. SAS Institute, March 2005. http://www.jmp.com

[4]   Laub, B., Thermal Protection Materials & Systems Branch, NASA Ames Reasearch Center. 55th Pacific Coast Regional and Basic Science Division Fall Meeting. Oakland, California. October 19-22, 2003.

[5]   Laub, B., et al. Thermal Protection System Technology and Facility Needs for Demanding Future Planetary Missions. International Workshop for Planetary robe Atmospheric Entry and Descent Trajectory Analysis and Science. Lisbon, Portugal. October 6-9, 2003.

[6]   Amundsen, Ruth M., et al. Thermal Analysis Methods for an Earth Entry Vehicle. Eleventh Thermal and Fluids Analysis Workshop. Cleveland, Ohio. August 21-25, 2000.

[7]   "General Purpose Thermal/Fluid Network Analyzer". SINDA/FLUINT V4.7 User's Manual. C&R Technologies

[8]   Dec, John. "CMA Fundamentals". Presented at STAB Thermal Group Review. March 01 2004.

[9]   Chen, Y.K., et al. "Ablation and Thermal Response Program for Spacecraft Heatshield Analysis". Thermal Protection Materials and Systems Branch. AIAA. 1997.

[10]   Laub, B. "Tutorial on Ablative TPS." Space Technology Division. NASA Ames. August 22, 2004.

[11]   Dec, John. "Probabilistic Design of a Mars Sample Return Earth Entry Vehicle Thermal Protection System." 40th Aerospace Sciences and Meeting & Exhibit. Reno, Nevada. January 14-17, 2002.

[12]   Braun, Robert, D.: "Planetary Entry, Descent, and Landing." Presentation, Georgia Institute of Technology, Atlanta, GA, 2004. Web-published: http://www.ae.gatech.edu/~rbraun/PlanetaryEDL.pdf

[13]   Kiper, J.D., et al. Assessing Usability off a Risk Based Requirements and Design Tool. Proceedings of the 7th IASTED International Conference, Software Engineering and Applications. November 3-5, 2003, Marina Del Ray, CA.

[14]   Feather, Martin S. "Mitigations and Their Attributes." DDP help files. DDP version 4-3-16.

[15]   Wilson, J.W., et al, "Collaborative Engineering Methods for Radiation Shield Design."   [http://lowdose.tricity.wsu.edu/2001mtg/abstracts/singleterry.htm. Accessed March 2005].

[16]   Collins,   E.M.,   "RAM   –   Rapid   Aircraft   Modeler," [http://www.erc.msstate.edu/~emc/projects/ram22/ . Accessed March 2005]

[17]   Wilson, J.W., Cucinotta, F.A., et al, "International Space Station Radiation Shielding Model Development," NASA-2001-01ICES-2370, 2001.

[18]   Wilson, J.W., Singleterry, R.C., Badavi, F.F., et al., "A Radiation Shielding Code for Spacecraft and its Validation," 44th International SAMPE Symposium and Exhibition, Long Beach, CA, May 23-27, 1999.

[19]   Wilson, J.W., Badavi, F.F., Cucinotta, F.A., Shinn, J.L, Badhwar, G.D., Silberberg, G., Tsao, C.H., Townsend, L.W., Tripathi, R.K., "HZETRN: Description of a Free-Space Ion and Nucleon Transport and Shielding Computer Program ," NASA TP-3495, May 1995.

[20]   Adams, J.H., "The Variability of Single Event Upset Rates in the Natural Environment," IEEE Transactions on Nuclear Science, Vol. NS-30, No. 6, Dec. 1983. pp. 4475-80.

[21]   Bendel, W.L. and Petersen, E.L., "Proton Upsets in Orbit," IEEE Transactions on Nuclear Science, Vol. NS-30, No. 6, Dec. 1983. pp. 4481-5.

[22]   Wilson, J.W., et al, "Effects of Target Fragmentation on Evaluation of LET Spectra From Space Radiation in Low Earth Orbit Environment: Impact on SEU predictions," 32nd Annual International Nuclear and Space Radiation Effects Conference, Madison, Wisconsin, July 17-21, 1995.